Screening for Biologically Annotated Drugs That Trigger Triacylglycerol Accumulation in the Diatom Phaeodactylum

Melissa Conte, Josselin Lupette, Khawla Seddiki, Coline Meï, Lina-Juana Dolch, Valérie Gros, Caroline Barette, Fabrice Rébeillé, Juliette Jouhet, Eric Maréchal

Short title

Drugs triggering oil accumulation in *Phaedactylum*

Title

Phenotypic screening of a biologically annotated drug library for the discovery of pathways involved in triacylglycerol accumulation in *Phaeodactylum*

Authors

Melissa Conte, Josselin Lupette, Khawla Seddiki, Coline Meï, Lina-Juana Dolch, Valérie Gros, Caroline Barette, Fabrice Rébeillé, Juliette Jouhet, Eric Maréchal*

Affiliation

Laboratoire de Physiologie Cellulaire et Végétale, CNRS, CEA, INRA, Université Grenoble Alpes, Institut de Biosciences et Biotechnologies de Grenoble, CEA-Grenoble, 17 rue des Martyrs, 38000 Grenoble, France

* correspondence: eric.marechal@cea.fr

One sentence summary

A phenotypic screen highlights drugs and endocrine disruptors triggering oil accumulation in *Phaedactylum* and points genes and pathways for future engineering strategies.

List of author contributions

M.C. performed most of the screening experiments; J.L., M.C and L.J.D. contributed to dose-response studies and phenotypic analyses; J.L., K.S. and E.M. contributed to whole genome transcriptomic analyses; V.G. provided technical assistance for lipidomic profiling; F.R. and J.J. provided specific expertise in glycerolipid analyses; C.B. provided specific expertise and technical assistance for phenotypic screens; E.M. conceived the project; all the authors contributed to the writing of the article.

Keyword

Phaeodactylum, diatoms, phenotypic screening, triacylglycerol, oil, lipids, small molecules, endocrine disruptors, estrogens, Ethynylestradiol

Abstract

Microalgae are a promising feedstock for the production of triacylglycerol (TAG) for a variety of applications. However, obtaining high TAG yields is challenging and novel strategies are needed. Approaches based on serendipity might accelerate the identification of unknown targets for improvements. A phenotypic assay was developed to screen a library of 1,200 drugs, annotated with pharmacology information, and select compounds triggering TAG accumulation in the diatom *Phaeodactylum*. We identified 34 hit molecules acting in a dose-dependent manner. Previously characterized targets of these compounds include cell division and cell signaling effectors, membrane receptors and transporters, and sterol metabolism. Among the five compounds possibly acting on sterol metabolism, we focused our study on Ethynylestradiol. This estrogen, used in contraceptive pills, is known for its ecological impact as an endocrine disruptor. Ethynylestradiol impaired the production of very-long chain polyunsaturated fatty acids (VLC-PUFA), destabilized the galactolipid vs. phospholipid balance and triggered a recycling of fatty acids (FA) from membrane lipids to TAG. *Phaeodactylum* transcriptomic response was consistent with a reallocation of carbon from sterols to acetyl-CoA and TAG. The mode of action and catabolism of Ethynylestradiol is unknown but might involve several upregulated cytochrome P450 proteins. A FA elongase, Delta6-ELO-B2, might be involved in the impairment of VLC-PUFA and FA turnover. This phenotypic screen opens new perspectives for the exploration of novel bioactive molecules, potential target genes and pathways. It also unraveled the sensitivity of diatoms to endocrine disruptors, highlighting an impact of anthropogenic pollution on phytoplankton, which should be considered in the future.

Introduction

Photosynthetic algae are promising systems for the biotechnological development of cell factories, since they are able to capture CO_2 and produce valuable biomolecules such as triacylglycerols (TAGs). Oils made of TAGs have a broad range of applications from feed, food or health, to commodity products complementing fossil hydrocarbons and chemistry (Lupette and Maréchal, 2018). TAGs contain three fatty acids (FA) esterified to a glycerol backbone, and they accumulate inside cells in the form of lipid droplets (LD) (Maeda et al., 2017). The potentiality of algal oil lies in the molecular variety of FAs esterified to TAGs, with chain lengths ranging from ~14 to ~22 carbons and harboring from 0 to 6 double bonds (Dolch and Marechal, 2015). Some examples of FAs are palmitic acid (16:0, with 16 carbon and no double bond), oleic acid (18:1), linolenic acid (18:3), eicosapentaenoic acid or EPA (20:5), etc. Very-long chain polyunsaturated FAs (VLC-PUFAs), like EPA, have a higher added value for food or health applications and shorter chained and less saturated FAs, such as 16:0, comply with biofuel applications (Lupette and Maréchal, 2018). Increasing the productivity and quality of alga-based oil are critical bottlenecks that need to be overcome (Pulz and Gross, 2004; Spolaore et al., 2006; Chisti, 2013; Klein-Marcuschamer et al., 2013; Ruiz et al., 2016; Arbenz et al., 2017).

The biodiversity of algae occupies very distant branches of the tree of life (Brodie et al., 2017), ranging from prokaryotes, *i.e.* cyanobacteria, to a multitude of eukaryote lineages, arisen either from a primary endosymbiosis, such as unicellular green algae, or from a secondary endosymbiosis, such as diatoms (Bozarth et al., 2009; Levitan et al., 2014). Important eukaryotic models with well annotated genomes, transformation techniques and molecular tools for genetic engineering are being developed, like *Chlamydomonas reinhardtii* for green algae (Merchant et al., 2007; Scaife and Smith, 2016), *Phaeodactylum tricornutum* for diatoms (Falciatore et al., 1999; Siaut et al., 2007; Bowler et al., 2008; De Riso et al., 2009; Daboussi et al., 2014; Nymark et al., 2016) or *Nannochloropsis* species for eustigmatophytes (Kilian et al., 2011; Anandarajah et al., 2012; Vieler et al., 2012; Corteggiani Carpinelli et al., 2014). The secondary endosymbionts have arisen from a complex evolutionary history (McFadden, 1999; Stoebe and Maier, 2002; Kutschera and Niklas, 2005; Gould et al., 2008; Keeling, 2009; Botte and Marechal, 2014; Petroutsos et al., 2014; Brodie et al., 2017); their subcellular ultrastructure is extremely sophisticated (Flori et al., 2016) and the annotation of their genome highlights a large proportion of proteins of unknown function compared to other eukaryotes originating from a primary endosymbiosis (Maier et al., 2000; Gardner et al., 2002; Armbrust et al., 2004;

Bowler et al., 2008; Deschamps and Moreira, 2012). Species such as *Phaeodactylum* and *Nannochloropsis* have cultivation and oil productivity performances complying with the development of production strains for industrial processes (d'Ippolito et al., 2015; Ajjawi et al., 2017; Wang and Seibert, 2017). Some rationalized approaches *via* genetic engineering require robust prior knowledge, in particular regarding the function of genes or pathways that might be modified in an attempt to drive carbon flux toward TAG production (Liao et al., 2016; Brodie et al., 2017). We need to advance our knowledge on the specific subcellular compartmentalization of secondary endosymbionts, cell growth and development, photosynthesis efficiency, CO_2 capture, carbon partitioning, glycerolipid metabolism etc., so as to develop strains and processes with higher biomass yields, TAG productivity and controlled FA contents.

Approaches based on serendipity might help accelerating the identification of still unknown targets for improvements. Phenotypic screens have been used to identify molecules that could trigger the accumulation of TAG in various microalgae strains, such as the green algae *Chlamydomonas*, *Chlorella* and *Tetrachlorella* (Wase et al., 2017) and secondary endosymbionts such as *Nannochloropsis* and *Phaeodactylum* (Franz et al., 2013). Having an active molecule in hand, it is then possible to search for the protein target(s) that could then be used to develop a genetically engineered strain, modified in the targeted pathway (Mayer et al., 1999; Haggarty et al., 2000; Marechal, 2008, 2009), however this molecule-to-target approach is long and uncertain. Here, we describe the screening of a biologically annotated library of compounds (or chemolibrary), containing drugs previously approved for safety by the U.S. food and drug administration for at least one indication or at least used in clinical trials with bioavailability, pharmacology and toxicity information (Prestwick Chemical Library; 1,200 compounds). The screen was developed to select molecules triggering the accumulation of TAG within *Phaeodactylum tricornutum* living cells. Theoretically, hit molecules from this repurpose collection should interact with *Phaeodactylum* proteins that share some structural and/or functional features with the original drug targets (Blagosklonny, 2003; Jeong et al., 2015; Coleman et al., 2016). Our objective was then to attempt identifying biological processes or pathways affected by the active molecules and propose lines of research for future *Phaeodactylum* strain developments.

Results

Setup of screening conditions and statistical robustness of the selected multi-parametric assay

Our objective was to define a multi-parametric assay allowing the robust measures of cell concentrations, TAG levels and ideally other parameters that would allow the monitoring of the physiological status of cells. We first optimized culture conditions for *Phaeodactylum* in different multiwell plate systems. After Pt1 wild type cells were dispensed in 48- or 96-well plates, manual observations were performed, highlighting an excess of adherent cells to the plastic sides in 96-well plates. In 48-well plates, addition of 4-mm glass beads helped limiting cell adhesions, aided mixing and allowed the detection of growth and of TAG accumulation after 48-hour incubations. We compared different methods to monitor cell abundance with sufficient high-throughput and statistical robustness. The easiest method would be by deducing cell abundance from light absorbance. We compiled data obtained from 140 independent data points, using *Phaeodactylum* cultures grown in plates or in flasks, in ESAW containing or lacking nitrogen (ESAW 1N1P or 0N1P, respectively). Cell concentrations were evaluated using a Malassez counting chamber. In this compiled dataset, a linear correlation was detected with absorbance measured at 730 nm (A_{730}), with the following equation: $y = 1.834.10^{-8}.x + 0.03758$ (correlation coefficient of 0.9637, Supplementary Fig S1). Unfortunately, in the conditions used for the screening, the dynamic range (difference between highest and lower value) was not sufficient. We tried to develop DAPI (4',6-diamidino-2-phenylindole) or Hoechst staining methods, based on the binding of these dyes to nuclear DNA, but the background was too strong to allow a statistically relevant determination of cell abundance. Eventually, we used a strain expressing an Histone H4 fused to EYFP (Enhanced Yellow Fluorescent Protein) at the N-terminus (Siaut et al., 2007), kindly provided by Angela Falciatore (Université Pierre et Marie Curie, Paris), allowing the determination of nuclei by exciting at 515 nm and measuring the emitted fluorescence at 530 nm. Using a calibrated culture with known cell concentrations, YFP fluorescence allowed evaluating cell abundance with a linear correlation coefficient of 0.97 (Figure 1A). This correlation is valid from 0.1 to 0.55 mM $NaNO_3$. In the same plates, it was therefore also possible to detect the fluorescence of chlorophylls and of Nile red, a dye binding to lipid droplets (Figure 1B and 1C), within a linear

range based on positive and negative cell controls, *i.e.* cells incubated for 48 hours in absence or in presence of nitrogen.

A statistical analysis classically used to determine the suitability of an assay is the *Z'* factor (Zhang et al., 1999), derived from measures obtained with positive and negative controls. Using our selected assay conditions and after 48-hour incubations, a series of low-TAG and high-TAG control cells were analyzed, *i.e.* 17 wells containing cells grown in 1N1P medium ($3.3.10^6$ cells.mL^{-1}) and 17 wells containing cells grown in 0N1P medium ($1.6.10^6$ cells.mL^{-1}) respectively (Supplementary Fig S2). Based on results, the *Z'* factor was calculated for cell abundance measures (based on YFP fluorescence), *i.e.* 0.75, TAG content (based on Nile Red fluorescence), *i.e.* 0.64 and chlorophyll level, *i.e.* 0.73. These values being > 0.5 indicated that the different conditions established during assay optimization have led to an accurate standardized assay, suitable for the search of new bioactive molecules from the screen of a chemical library.

Primary and secondary screens to identify molecules triggering TAG accumulation in *Phaeodactylum*

The screening of the Prestwick Chemical Library (1,200 compounds) was performed at a final concentration of 10 µM and 0.5% DMSO, using the automated multi-module platform from the CMBA (Centre de criblage pour des molecules bio-actives), Grenoble. Thirty plates could be analyzed per week. Combined data are shown in Figure 2.

Two main criteria were used to select compounds for a secondary screen. First criterion was a low impact on cell growth, viability and chlorophyll level. Chlorophyll fluorescence level correlated linearly with cell abundance, with a correlation coefficient of 0.8189 (Figure 3A). About 20% of the compounds were lethal for *Phaeodactylum* at 10 µM, with YFP fluorescence lower than 10% of control. Some compounds had apparently no impact on cell abundance but led to a strong decrease of chlorophyll, below 50% of control level. These compounds were not considered further. Second criterion was an increase in TAG level. A list of 160 compounds leading to an increase in Nile Red staining above 120 % of average per plate, while maintaining a cell abundance above 50 % of control (Figure 3B) were then selected.

A secondary screen of the 160 compounds consisted in a re-evaluation of their effect at 10 µM, in the same conditions and in technical duplicates, so as to discard a first series of false positives and rank compounds (Figure 3C). A list of 40 compounds was then tested in independent

biological triplicates, so as to select a series of 34 hit molecules showing an increase in Nile Red higher than 120% (and up to 385%) (Table 1).

Previously characterized targets of the selected compounds were classified based on general biological function and/or molecular features and highlighted seven major categories of targets: (1) nucleic acid biosynthesis and cell division (Pentamidine, Oxytetracycline, Ifosfamide, Rifaximin and Nocodazole); (2) membrane receptors (Xylometazoline, Labetalol, Acebutolol, Meclizine, Serotonin, Alverin, Pirenperone, Hyoscyamine, Pipenzolate, Mecamylamine, Bephenium and Dimaprit); (3) membrane transporters (Bendroflumethiazide, Rimantadine, Gaboxadol and Antimycin A); (4) sterol metabolism (Estrone, Ethynylestradiol, Mevastatin, Simvastatin and Ketoconazole); (5) cyclic nucleotide signaling (Zardaverine and Trapidil); (6) oxylipin signaling (Meloxicam, Azapropazone and Misoprostol) and eventually (7) unrelated enzymes involved in carbohydrate metabolism, purine catabolism and/or beta-lactam drug resistance (Miglitol, Flucloxacillin, Sulbactam and Allopurinol) (Table 1). In addition, we examined possible side-effect on secondary targets and noticed that six compounds could have pleiotropic effects and act on cytochrome P450 enzymes involved in sterol metabolism (Table 1). The consistency of the possible target categories or pathways, which are hit by the selected molecules is striking and supports the biological relevance of the obtained results.

Only 5 compounds triggered an increase in Nile Red staining in all independent biological triplicates, and with an apparent low toxicity, *i.e.* Nocodazole, Antimycin A, Ethynylestradiol, Mevastatin and Allopurinol.

Dose-response analyses of hit molecules triggering TAG accumulation in *Phaeodactylum*

Focusing on the 5 molecules selected following primary and secondary screens, we performed a tertiary test, consisting in dose-response analyses, in triplicates, at compound concentrations of 1.5, 3, 6, 12, 25, 50 and 100 µM (Figure 4). The first striking observation is that besides Nocodazole, selected molecules appear to impair growth at high concentrations, above 25-50 µM, based on cell abundance measured via the fluorescence of Histone H4 protein fused to EYFP. Three compounds triggered a regular increase in TAG per cell, in the tested range (Antimycine A, Ethynylestradiol and Allopurinol), whereas the increase in Nile Red fluorescence observed with Mevastatin and Nocodazole reached a limit at 50 µM. The accumulation of TAG appears therefore to be correlated with the concentration of molecules in the 10-micromolar range.

This dose-response analysis supports the activity of selected compounds triggering TAG accumulation in *Phaedoctylum*, likely *via* the interference of mitochondria and/or chloroplast electron transport chain (Antimycine A), microtubule dynamics (Nocodazole), sterol metabolism (Ethynylestradiol and Mevastatin) and purine catabolism (Allopurinol).

Chemical interference of sterol metabolism.

The screen highlighted compounds potentially targeting enzymes of the mevalonate pathway and sterol metabolism, from the most upstream enzymes, such as the hydroxymethylglutaryl-CoA reductase (or HMG-CoA reductase) hit by Simvastatin and Mevastatin, to downstream enzymatic activities, such as a sterol 14-alpha demethylase hit by Ketoconazole. This latter compound proved to be toxic at concentrations higher than 30 µM. We analyzed additional molecules known to interfere with this pathway (Figure 5). The biosynthesis of isopentenyl-pyrophosphate (isopentenyl-PP) and farnesyl-pyrophosphate (farnesyl-PP) is common to all isoprenoids, whereas the biosynthesis of squalene is specific to sterol biosynthesis. Risedronate, known to inhibit farnesyl pyrophosphate synthase (Bergstrom et al., 2000) triggered an increase in TAG when provided at concentrations higher than 30 µM. We confirmed that Ro48-8071, an oxydosqualene cyclase (OSC) inhibitor, induced an accumulation of TAG, as previously described (Fabris et al., 2014). The accumulation of TAG was observed when Ro48-8071 was supplied at 3 µM, whereas above 30 µM this compound was toxic. Figure 5 also shows the possible interference of cytochrome P450 oxidases/hydroxylases acting downstream in the sterol pathway, which could be inhibited by Ethynylestradiol, Ifosfamide, Labetalol, Acebutolol and Meloxicam (see also Table 1). Following our screening, the high proportion of inhibitors of sterol metabolism highlights therefore that this pathway represents a strong competitive route, diverting acetyl-CoA from fatty acids and TAG. This proportion of sterol metabolism antagonists could also reflect a bias in the library of compounds we screened. Interestingly, although high concentrations of molecules impaired growth, lower concentrations triggered an increase in TAG with a low impact on cell proliferation.

Lipidomic remodeling and physiological response induced by Ethynylestradiol

A previous genetic study had demonstrated that the impairment of sterol metabolism, following the downregulation of one of its enzymes, OSC, led to an interruption of the sterol biosynthetic pathway and a strong increase in Nile Red fluorescence, suggesting an accumulation of TAG in *Phaeodactylum* (Fabris et al., 2014). However, the precise remodeling of glycerolipids and its mechanism had not been precisely analyzed. The increase in TAG proportion was not

characterized and it was not established whether all membrane glycerolipids were altered, regardless of their fatty acid molecular species or their polar heads, or if a specific tuning could operate (Fabris et al., 2014).

We focused our analyses on Ethynylestradiol (structure, also named 17-α-Ethynylestradiol or EE2) (Inhoffen and Hohlweg, 1938), since this compound was effective at low concentrations, is supposed to act downstream in the pathway and is one of the most soluble molecules we identified. Ethynylestradiol is a synthetic estrogen that could mimic potential analogs acting as natural hormones/pheromones/infochemicals. It is a derivative of Estrone, used in birth control pills, based on its higher binding affinity to the human estrogen receptor (Jensen and DeSombre, 1973). This compound has recently attracted an increasing attention since both natural and synthetic estrogens are discharged in the environment by anthropogenic practices, including human and domestic animals (Aris et al., 2014; Adeel et al., 2017). Estrogens have demonstrated impacts on the aquatic environment, including a well-studied effect on sex determination in fish (Bhandari et al., 2015; Siegenthaler et al., 2017), however the effects of these endocrine disruptors on phytoplankton have been very poorly investigated (Liu et al., 2010; Pocock and Falk, 2014).

First, we checked that the estimate of cell abundance based on Histone 4-YFP fusion was accurate: we repeated the dose-dependent experiment, confirming that Nile Red staining increased regularly with increasing doses of Ethynylestradiol, and reevaluated cell numbers using a Malassez counting chamber (Supplementary Figure S3), confirming that Ethynylestradiol had a significant impact on growth at concentrations higher than 8-10 µM. The cells did not show any strong defect at the level of photosynthesis, based on photosystem II efficiency measured by the *Fv/Fm* ratio, besides a moderate decline above 30 µM (Supplementary Figure S3).

We then sought to confirm whether the increased Nile Red staining level corresponded to a significant change in TAG. To that purpose, we determined the glycerolipid profile of *Phaeodactylum* cells, grown in 400 mL of 1N1P medium, 0.5% DMSO in presence or absence of Ethynylestradiol 30 µM and at a cell density of 1.10^6 cells.mL^{-1}. After a 48-hour incubation, glycerolipids were extracted and analyzed as described previously (Abida et al., 2015). Major polar glycerolipids consist of a glycerol backbone to which 2 fatty acids are linked by ester bonds and harboring a polar head. In *Phaeodactylum*, chloroplast-specific classes comprise acyl-sulfoquinovosyldiacylglycerol (ASQ), sulfoquinovosyldiacylglycerol (SQDG),

monogalactosyldiacylglycerol (MGDG), digalactosyldiacylglycerol (DGDG) and phosphatidylglycerol (PG). Glycerolipids synthesized by the endoplasmic reticulum comprise phosphatidylcholine (PC) and diaclyglycerylhydroxymethyl-N,N,N-trimethyl-β-alanine (DGTA) (Abida et al., 2015). Following the treatment with Ethynylestradiol, a strong increase in TAG could be observed, confirming Nile Red staining increase (Figure 6, A, left). Polar lipids were apparently not strongly affected besides a specific decrease in MGDG and an increase in PC. Interestingly, similar trends were observed after a treatment with 15 µM Simvastatin, another molecule targeting sterol metabolism (Figure 6, A, right).

When analyzing fatty acid profiles within each class of glycerolipids, striking differences could be observed. Firstly, with the noticeable exception of SQDG, the proportion of eicosapentaenoic acid or EPA (20:5) decreased in all major lipid classes, *i.e.* MGDG, DGDG, PG, PC, DGTA (Figure 6, B). The synthesis of this VLC-PUFAs is still not completely elucidated, but it is now considered that it is elaborated from short-chain fatty acids, including saturated molecular species such as 16:0 (Dolch et al., 2017), by a series elongations and desaturations (Sayanova and Napier, 2004; Dolch and Marechal, 2015; Sayanova et al., 2017). The elongation occurs on FAs linked to co-enzyme A (as acyl-CoAs), whereas desaturations should occur on FAs linked to a membrane lipids, possibly PC and/or DGTA in *Phaeodactylum* (Dolch and Marechal, 2015; Sayanova et al., 2017). The process is so fast that the unsaturated FA precursors of 20:5 (*i.e.* 20:4, 20:3, 18:4, 18:3, 18:2, 18:1) are barely detected in *Phaeodactylum* and represent a few percent. Following treatment with Ethynylestradiol, the decrease in 20:5 coincides with a decrease of 20:4 and an increase of the proportion of their unsaturated FA precursors, in both PC (18:4, 18:3, 18:2, 18:1) and DGTA (18:4, 18:3, 18:2). Ethynylestradiol appears therefore to specifically disturb the channeled production of 20:5 *via* these two lipids, and supports that both PC and DGTA can be platform lipids for the elaboration of EPA in *Phaeodactylum*.

In parallel to this alteration of FA elongation and desaturation generating VLC-PUFAs, TAG content increased (Figure 6, A, left). TAG profile was modified, with higher proportions in FAs deriving from membrane lipids, such as 16:1 and 20:5, and including unsaturated FAs, which are uncommon in *Phaeodactylum* TAG, such as 16:2, 16:3, 18:4 (Figure 6, C). Altogether, these results indicate that Ethynylestradiol impairs EPA elaboration *via* PC and DGTA, destabilizes MGDG/PC balance and triggers a turnover of FAs deriving from membrane lipids to TAG.

Transcriptomic reprogramming induced by Ethynylestradiol.

The striking modification of the glycerolipid profile, showing an unsuspected disruption of EPA biosynthesis and a strong reallocation of carbon suggested that *Phaedoctylum* might operate an important transcriptomic reprogramming. *Phaeodactylum* cells were therefore treated for 4 days in independent biological triplicates with 0, 10 and 20 µM of Ethynylestradiol, conditions known to trigger TAG accumulation with moderate impact on growth (Supplementary Figure S4). Following treatment, frozen cells (2.10^8 cells) were used to extract and purify 10-20 µg RNA per sample, and RNAseq analysis was performed with an Illumina Hiseq 4000 system (20 Million reads). Reads were mapped on the genome of *Phaeodactylum tricornutum* using the Star (Spliced Transcripts Alignment to a Reference) method (Dobin et al., 2013; Engstrom et al., 2013). Data were filtered based on the detection of 1 read in at least one sample per treatment or genomic mutation and then normalized using the DESseq2 method (Varet et al., 2016) (Supplementary Table S1).

We found 962 genes differentially expressed with a |Log2(fold change)| > 1 in at least one of the contrasts (i.e. comparing Ethynylestradiol supplies at 0 µM vs. 10 µM, 0 µM vs. 20 µM or 10 µM vs. 20 µM), and with p-value lower than 0.05. A partition of differentially expressed genes was performed using a *K-mean* method, with the number of partitions set to 6 (Liu et al., 2014; Dolch et al., 2017). Each group or cluster consisted of genes with similar expression profiles following treatments with Ethynylestradiol (Figure 7). Two clusters comprise genes downregulated following treatments, i.e. group 1 (DR_1) gathering genes with the strongest magnitude in expression decline (in the -2 to -4 Log2FC range) and group 5 (DR_2) with moderate but significant expression decline (Log2FC ~ -1 to -2). Four clusters comprise genes upregulated following Ethynylestradiol treatments, i.e. groups 2, 3, 4 and 6 (UR_1, UR_2, UR_3 and UR_4, respectively), UR_1 and UR_3 in the most moderate change levels (Log2FC ~ 1), UR_2 and UR_4 with the highest variation magnitude (Log2FC ~ 2 to 4).

For each group we sought whether gene ontology (GO) terms could be enriched, using the GOseq R package, with p-values lower than 0.05 or 0.1 (Young et al., 2010) (Supplementary Table S2). We then mined results, focusing on carbon metabolism, ***i.e.*** the putative enrichment of GO terms corresponding to the glycolysis, phosphoenolpyruvate production, pyruvate production, acetyl-CoA production, mevalonate pathway and glycerolipid production (Supplementary Table S2).

- UR_1 was characterized by a moderate enrichment in genes involved in lipid biosynthesis (p-value < 0.1).

- A GO enrichment in terms corresponding to the mevalonate pathway was clearly observed in UR_2 cluster, both at the molecular function (diphosphomevalonate decarboxylase activity; p-value < 0.05) and biological process (isopentenyl diphosphate biosynthetic process, mevalonate pathway; p-value < 0.05) levels. UR_2 cluster was also enriched in GO terms corresponding to glycolysis and pyruvate metabolism with a p-value < 0.1, lipid metabolism.
- UR_3 was not enriched in GO terms corresponding to carbon metabolism.
- UR_4 cluster was also enriched in GO terms corresponding to acetyl-CoA biosynthesis from pyruvate (p-value < 0.05).
- In down-regulated clusters, DR_1 did not shown any clear enrichment in GO terms linked to carbon metabolism, whereas DR2 showed an enrichment in terms corresponding to gluconeogenesis (p-value < 0.05).

This analysis of the function of genes differentially expressed highlights therefore that glycolysis was likely stimulated, whereas neoglucogenesis was arrested, and that the mevalonate pathway was up-regulated, consistent with a response to an agent blocking sterol metabolism. Genes involved in carbon metabolism appears also tuned toward the production of acetyl-CoA from pyruvate, which was then directed toward fatty acids and lipids.

We examined therefore more carefully the corresponding metabolic pathways. It has been demonstrated that the isopentenyl-diphosphate precursor used for sterol biosynthesis derives from the cytosolic Mevalonate pathway rather than the plastid localized 1-Desoxy-D-xylulose-5-phosphate (or DOXP) pathway (Cvejic and Rohmer, 2000). Supplementary Table S3 shows therefore the dose-dependent response of genes involved in sterol biosynthesis, first via the Mevalonate route: in the most upstream section of the pathway, the expression of the HMG-CoA synthase gene, *HMGS* (Phatr3_J16649), increased in a dose-dependent manner, whereas the expression of the mevalonate kinase gene, *MK* (Phatr3_J53929) was strongly attenuated. One gene coding for a putative Geranyl-diphosphate synthase, GPPS (Phatr3_J47271) was strongly down-regulated whereas a Geranyl-diphosphate/Farnesyl-diphosphate synthase, *GPP-FPPS* (Phatr3_J49325) was up-regulating, illustrating the fine tuning of different redundant enzymes within the sterol pathway, likely involved in specific physiological or developmental processes. In the most downstream part of the pathway, the genes coding for the putative 14-alpha-demethylase, *CYP51* (Phatr3_J31339), 3-beta-hydroxysteroid-delta(8), delta-7-isomerase (Phatr3_J36801), delta-7-sterol delta-5-dehydrogenase (Phatr3_J14208), delta-7-sterol reductase (Phatr3_J30461) and sterol C-22 desaturase, *CYP710* (Phatr3_J51757) were

strongly upregulated in a dose-dependent manner by the treatment with Ethynylestradiol. Interestingly, genes coding for cytochrome P450 enzymes, possibly targeted by Ethynylestradiol (most importantly *CYP710*) were therefore strongly activated. We wondered whether the expression of genes involved in the production of isopentenyl-diphosphate *via* the DOXP pathway could also be altered by the treatment, but no specific change could be detected (Supplementary Table S3). The reprogramming of sterol biosynthesis genes combines therefore an activation of genes of the *CYP* family possibly compensating the inhibition by Ethynylestradiol, whereas others, most importantly *MK*, act like general bottlenecks and possibly reduce the flux of carbon through this pathway.

In Supplementary Table S4, we analyzed genes involved in glycerolipid metabolism. Surprisingly, only a few genes involved in FA and TAG biosynthesis were upregulated. Consistently with an increase in acetyl-CoA production for FA synthesis, we noticed for instance that genes coding for Dihydrolipoamide acetyltransferase components of pyruvate dehydrogenase complex (Phatr3_J23850, Phatr3_EG02309, Phatr3_J30113) and for the Biotin carboxylase subunit of heteromeric acetyl-CoA carboxylase (Phatr3_J49339) were upregulated. At the level of TAG biosynthesis, only one of the diacylglycerol acyltransferase (*DGAT2C*) genes was upregulated (Phatr3_J31662). By contrast, at the level of TAG degradation, the expression of lipases was strikingly downregulated, *i.e. MAGL1* (Phatr3_J43352), *SDP1-Like* (Phatr3_J45518), *TAGL-Like-A* (Phatr3_J1971), *PLA-A* (Phatr3_J44005), *PLA-B* (Phatr3_J44066) and *Patatin-like-A* (Phatr3_J43678). Likewise, genes involved in FA beta-oxidation in both the peroxisome (Phatr3_J19979, Phatr3_J41969, Phatr3_J45947, Phatr3_J11319, Phatr3_J37372 and Phatr3_J31367) and the mitochondrion (Phatr3_J20310, Phatr3_J35240, Phatr3_J40988, Phatr3_J11811, Phatr3_J54494, Phatr3_J18064) were down-regulated. Altogether, the transcriptomic reprogramming in response to Ethynylestradiol highlights a downregulation of genes involved in TAG catabolism, rather than a strongly enhanced TAG biosynthesis, suggesting that TAG turnover was slowed down in response to the chemical treatment.

Focusing on VLC-PUFAs, most genes involved in the biosynthesis of EPA (*Delta0-ELO-A*, Phatr3_J49867; *Delta0-ELO-B*, Phatr3_J16376; *Delta5-ELO-B*, Phatr3_J34485; *Delta5-ELO-A*, Phatr3_J9255; *Delta6-ELO-B2*, Phatr3_J20508; *HACD*, Phatr3_J44831; *ER-delta5-FAD-A*, Phatr3_J46830; *ER-delta5-FAD-B*, Phatr3_J22459 and *ER-delta6-FAD*; Phatr3_J29488) were up-regulated. Only one of the genes was downregulated, coding for Delta6-ELO-B2 (Phatr3_J22274) (Supplementary Table S4). This disturbed VLC-PUFA coincides with the

upregulation of the betaine lipid synthase, *BTA-Like* (Phatr3_J42872), involved in the biosynthesis of DGTA (Supplementary Table S4).

Taken altogether, the transcriptomic response is therefore consistent with the observed phenotype and highlights possible genes, which coordinated regulation could lead to a strong modification of the FA profiles in important membrane lipids (PC, DGTA), a modulation of the MGDG/PC ratio and a carbon reallocation toward TAG, by preventing TAG catabolism. This scheme is very different from the transcriptomic reprogramming and lipid remodeling following nitrogen or phosphorus starvation, considered as a reference for industrial developments, in which TAG accumulates mainly following an orchestrated induction of FA synthesis genes and of multiple enzymes involved in TAG biosynthesis (Abida et al., 2015; Alipanah et al., 2015; Levitan et al., 2015).

Discussion.

Consistency of the screen and identification of candidate biological processes influencing triacylglycerol level in *Phaeodactylum*

The use of an annotated library of compounds, *i.e.* containing small molecules previously characterized on known targets, allows a rational analysis of screening outputs and a more rapid deduction of target candidates compared to screenings of large scale libraries containing tens of thousands of unannotated molecules. Here, we could screen 1,200 compounds of the Prestwick Chemical Library, using a multiparameter assay allowing the evaluation of cell abundance, TAG level and chlorophyll fluorescence (Figure 1) with appropriate statistical robustness based on *Z'* values. Possible biases or conditions leading to false positive or negative results have to be considered. An important bias lies in the choice of the library of compounds, which could be enriched in drugs developed to act on specific human pathogeneses, such as molecules binding on neurotransmitter receptors, being effective on metabolic disorders, on cancer or on specific infectious diseases. This bias is a limitation on the number of target classes we can explore, but it can also be considered an advantage to identify molecules hitting a pathway at the level of multiple target enzymes. The miniaturized assay developed to measure whole cell responses, therefore allowing a selection of compounds that are actually active on the phenotype, can also produce false positive or negative results. The parameter used to estimate cell abundance was based on the fluorescence of Histone H4 fused to YFP, correlating linearly with cell counting from 0.1 to 0.55 mM $NaNO_3$ (Figure 1 and Supplementary Figure S1). Cell abundance could therefore be underestimated in conditions limiting protein biosynthesis. We therefore confirmed variations of cell abundance following treatments with selected molecules using a Malassez counting chamber (e.g. Supplementary Figure S3). Another important source of erroneous results lies in the use of Nile Red to stain TAG droplets: Nile Red staining allows relative comparisons within a batch of experiments and can react with other non-polar lipids. We therefore sought to confirm the observed increase of Nile Red staining obtained following selected chemical treatments by direct analysis of glycerolipids.

Our primary screen of 1,200 compounds was performed by incubating *Phaedocatylum* in presence of molecules supplied at 10 µM during 48 hours (Figure 2). We selected 160 compounds leading to an increase in Nile Red staining above 120 % of average per plate, while maintaining a cell abundance above 50 % of control (Figure 3) and we repeated the screen to discard false positives. A list of 40 molecules was then selected and tested in independent triplicates, and we selected the most active molecules in at least two of the three independent

assays. This secondary screen allowed the final selection of 34 hit molecules (Table 1). The success of a screening can be evaluated if some of the selected molecules have close chemical structures (showing consistency in the detection of an active chemical scaffold) or if distinct molecules hitting the same biological pathway are selected. Here, the screen pointed a very limited number of biological processes or pathways, *i.e.* nucleic acid biosynthesis and cell division, membrane receptors and transporters, cyclic nucleotide or oxylipin signaling and eventually sterol metabolism (Table 1). The consistency of the screen was further illustrated by the presence of similar chemical structures: Simvastatin and Mevastatin share a common 'statin' scaffold; Estrone and Ethynylestradiol are both estrogens, Serotonin is the ligand of serotonin receptors whereas Alverin and Pipenperone are both antagonists of the same receptor. The results of this screen evidently pointed towards sterol metabolism.

Five molecules were selected based on the detection of their bioactivity in all of the tests, likely interference with mitochondria and/or chloroplast electron transport chain (Antimycine A), microtubule dynamics (Nocodazole), sterol metabolism (Ethynylestradiol and Mevastatin) and purine catabolism (Allopurinol). We confirmed that the increase in Nile Red staining was dose-dependent (Figure 4), with an arrest of growth induced at concentrations higher that 10 to 50 µM, depending on the molecules. Thus, the screen has not allowed for the discovery of molecules that would combine an activation of TAG accumulation with a complete harmlessness. This indicates that the molecules might hit vital targets and/or that high doses increase unspecific toxicity. The advantage of using chemicals over conventional genetics is well known when addressing the question of essential proteins: one can study a phenotypic response at sub-lethal concentrations, decrease the activity of the target of interest with different magnitudes, trigger the phenotypic response at any developmental stage by simply adding the compound and eventually combine with other molecules or genetic backgrounds (Soleilhac et al., 2010). In addition, the chemical structure of selected molecules might be close enough to natural molecules to suggest a mimicry of a natural signaling process.

The output of the screen is also consistent with some previous studies showing an increase of TAG, (i) after the impairment of microtubule dynamics (using Taxol) and cell division in *Arabidopsis* cells (Meï et al., 2017), (ii) after the chemical inhibition or genetic knock down of sterol metabolism enzymes in *Phaeodactylum* (Fabris et al., 2014) or (iii) after incubation with nitric oxide ($NO^{\bullet}$) (Dolch et al., 2017), a known activator of nucleotide cyclases, opposing cyclic nucleotide phosphodiesterases (Francis et al., 2010). Focusing on compounds acting on sterol metabolism, we expanded our tests to additional molecules that were not initially

screened, known to act at the level of other enzymes of the pathway (Figure 5), and confirmed that carbon partitioning respected a balance between this pathway and TAG net production. The consistency of the screen suggests therefore that all biological processes we highlighted are promising for more in depth investigations.

Focused analysis of *Phaeodactylum* response to Ethynylestradiol.

Ethynylestradiol (19-nor-17α-pregna-1,3,5(10)-trien-20-yne-3,17-diol) is a synthetic derivative of the natural hormones Estrone and Estradiol (Inhoffen and Hohlweg, 1938). The presence of the ethynyl group makes this estrogenic steroid more resistant to oxidation and stable in the environment, with a half-life higher than 100 days in water, under aerobic conditions (Adeel et al., 2017). Water solubility of Ethynylestradiol is 16 mM at 20°C and the logarithm of its n-octanol/water partition coefficient (or log*P*) is 3.63 (Adeel et al., 2017), indicating a strong efficiency in crossing cell barriers (Lipinski et al., 2001). Used in birth control pills (Jensen and DeSombre, 1973), Ethynylestradiol binding affinity to the estrogen receptor is two times higher in humans and up to five times higher in some fish species, compared to natural hormones (Aris et al., 2014). Both natural and synthetic estrogens are considered as extremely alarming endocrine disruptors, following their discharge in the environment by anthropogenic practices (Aris et al., 2014; Adeel et al., 2017). High Ethynylestradiol concentrations have an impact on sex determination in some fish species (Bhandari et al., 2015; Siegenthaler et al., 2017). Our knowledge on the effects of estrogen on phytoplankton is very scarce, with only two reports regarding a negative impact on growth in the green alga *Chlamydomonas reinhardtii* (Pocock and Falk, 2014) and in the pennate diatom *Navicula incerta* (Liu et al., 2010). Interestingly, treatment with ~10 µM Ethynylestradiol triggered an increase in total acyl-lipids in *Navicula* (Liu et al., 2010), possibly due to the increase in TAG observed here in *Phaeodactylum*. In addition, a bioaccumulation of Ethynylestradiol was observed in *Navicula* (Liu et al., 2010; Liu et al., 2012), supporting that diatoms could concentrate this molecule over time. The study of the effect of high concentrations of molecules, ***i.e.*** an acute exposure, could therefore mimic the physiological situation after a long term exposure to low doses.

The mode of action of Ethynylestradiol in *Phaeodactylum* is unknown, however the past reports of inhibition of cytochrome P450 enzymes involved in sterol metabolism (Table 1, Figure 5) and the upregulation of *CYP* genes (Supplementary Table S3) suggest that one or more CYP proteins might be targeted. The biodegradation of Ethynylestradiol by *Navicula* (Liu et al.,

2010), also suggests that some CYP enzyme(s) might eventually use this estrogen as a substrate, leading to its bioconversion into a non-active compound. Thus diatoms might contribute to reducing the environmental concentration of this endocrine disruptor and decrease the detrimental impact on other aquatic species feeding on diatoms (Liu et al., 2012).

The phenotypic response to Ethynylestradiol is marked by a strong accumulation of TAG, which does not seem to balance a dramatic decline of polar lipid quantities, besides a moderate decrease in MGDG (Figure 6). This response suggest that TAG might simply accumulate following the disturbance of sterol biosynthesis, leading to an accumulation of acetyl-CoA diverted toward FA and TAG biosynthesis. This quantitative reallocation of carbon from one sink (sterols) to another (TAG) is supported by the upregulation of genes involved in acetyl-CoA biosynthesis and downregulation of genes involved in TAG degradation (Table S4). However, the analysis of FA within each class of glycerolipids showed striking differences, including in membrane glycerolipids, in particular a decrease of 20:5 proportion in all major lipid classes, *i.e.* MGDG, DGDG, PG, PC, DGTA (Figure 6, B). The synthesis of 20:5 starts in the endoplasmic reticulum from short-chain acyl-CoAs, including saturated molecular species such as 16:0 (Dolch et al., 2017). It proceeds by a series elongations of acyl-CoAs and of desaturation on FAs linked to a membrane lipids, possibly PC and/or DGTA (Sayanova and Napier, 2004; Dolch and Marechal, 2015; Sayanova et al., 2017). Elongation includes Δ0-ELOs (16:0 $\rightarrow$ 18:0) and Δ6-ELOs (18:3 $\rightarrow$ 20:3) (Dolch et al., 2017). Ethynylestradiol treatment induced an increase of the proportion of 20:5 unsaturated FA precursors, in both PC (18:4, 18:3, 18:2, 18:1) and DGTA (18:4, 18:3, 18:2), before the elongation by a Δ6-ELO. Consistently, although most genes involved in 20:5 biosynthesis are upregulated, including the gene coding for the betaine lipid platform on which desaturation occurs, *Delta6-ELO-B2* (Phatr3_J22274) is strikingly downregulated (Supplementary Table S4). This result suggests that a transcriptomic control of *Delta6-ELO-B2* likely occurs in response to Ethynylestradiol. This mechanism might therefore be an additional mechanism altering glycerolipids following treatments with estrogens.

Concluding remarks.

This study allowed the identification of molecules that could be of interest for a direct implementation in an industrial process aiming at triggering the accumulation of TAG in diatoms, which would be distinct from established methods such as nutrient starvation (Abida et al., 2015). An advantage is to determine cultivation conditions allowing the accumulation of

TAG with lower impact on growth. The use of an annotated library of compounds allowed for the identification of some metabolic pathways that might be scrutinized in more details for genetic engineering strategies in the future. Some of the identified pathways confirm past studies, such as nucleotide syntheses and cell division processes (Kim et al., 2017; Meï et al., 2017; Prioretti et al., 2017), sterol metabolism (Fabris et al., 2014; Gallo et al., 2017) or indirectly nitric oxide signaling (Dolch et al., 2017). Other remarkable biological processes highlighted here, involving membrane receptors and transporters or oxylipin signaling, now need to be investigated. The identification of compounds interfering with catecholamine metabolism, known to interfere with lipolysis in humans (Camell et al., 2017), raises the puzzling question of an analogous system in diatoms.

The discovery of two endocrine disruptors (Ethynylestradiol and Estrone) among the 5 more active molecules is one of the major results of this study. Ethynylestradiol has been reported to be used in aquaculture to develop single-sex populations of fish (Aris et al., 2014). Our study shows that these compounds have potentially a strong impact on phytoplankton as well, which needs now to be addressed in environmental contexts. On the one hand, the mode of action likely implies an interference of the metabolism in *Phaeodactylum*, possibly *via* the inhibition of one or more CYP enzyme(s) and the reallocation of carbon from one sink (sterols) to TAG. On the other hand, VLC-PUFA biosynthesis is strikingly impaired, following the downregulation of a gene involved in 18- to 20-carbon acyl elongation. This latter effect indicates that a specific transcriptomic control of VLC-PUFA biosynthesis is activated by estrogens. Treatment with Ethynylestradiol might therefore interfere with a process occurring in response to a natural sterol, either in an intracellular or a cell-to-cell signaling process. Although natural doses of Ethynylestradiol have not been measured systematically in the past, with some reports indicating ~15 pM in sea water (Adeel et al., 2017), the capacity of pennate diatoms to accumulate estrogens (Liu et al., 2010; Liu et al., 2012) gives relevance to study following acute exposures. Future works are therefore needed to address the question of the physiological processes chemical impaired by synthetic estrogens, and to address the environmental consequences of the response of diatoms detailed here.

Material and Methods

Chemicals and Library of small molecules

Chemicals used in the composition of growth media and solvents were obtained from Sigma-Aldrich. The Prestwick Chemical Library of 1,200 compounds was obtained from Prestwick Chemical (Illkirch-Graffenstaden, France) and consists exclusively of FDA (U.S. food and drug administration) approved compounds. The chemical library was stored at -20°C at a 10 mM concentration in 100% dimethylsulfoxyde (DMSO) and 50 µL-working solutions were prepared in 48 well plates before screening.

Cultivation of Phaeodactylum tricornutum

Experiments were performed with the *Phaeodactylum tricornutum* (Pt1) Bohlin Strain 8.6 CCMP2561 (Culture Collection of Marine Phytoplankton, now known as NCMA: National Center for Marine Algae and Microbiota) and with PtYFP, a strain expressing an Histone H4 fused to EYFP (Enhanced Yellow Fluorescent Protein) at the N-terminus, kindly provided by Angela Falciatore (Université Pierre et Marie Curie, Paris) (Siaut et al., 2007). *P. tricornutum* cells were maintained and grown in 50 mL at 20°C, in 250 mL flasks, in a modified ESAW (Enriched Seawater, Artificial Water) medium (NaCl 362.7 mM; Na_2SO_4 25 mM; KCl 8.03 mM; $NaHCO_3$ 2.067 mM; KBr 0.725 mM; H_3BO_3 0.372 mM; NaF 0.0657 mM; $MgCl_2$ 47.18 mM; $CaCl_2$ 9.134 mM; $SrCl_2$ 0.082 mM; Na_2-glycerophosphate 21.8 µM; Na_2SiO_3 105.6 µM; Na_2EDTA 14.86 µM; $Fe(NH_4)_2(SO_4)_2$ 5.97 µM; $FeCl_3$ 0.592 µM; $MnSO_4$ 2.42 µM; $ZnSO_4$ 0.254 µM; $CoSO_4$ 0.0569 µM; Na_2MoO_4 0.52 µM; H_3BO_3 61.46 µM; Na_2SeO_3 10 nM; biotin (vitamin H) 8.18 nM; cobalamin (vitamin B12) 2.94 nM; thiamine (vitamin B1) 0.594 µM) (Falciatore et al., 2000), using either 0.55 mM $NaNO_3$ and $2.2.10^{-2}$ mM NaH_3PO_4, or ten times enriched nitrogen and phosphate sources ("ESAW 10N10P", containing 5.5 mM $NaNO_3$ and 0.22 mM NaH_3PO_4) (Abida et al., 2015). Cells were grown on a 12 hour / 12 hour - light (50 $\mu mol.m^{-2}.s^{-1}$) / dark cycle. Cells were sub-cultured twice a week by inoculating 10^6 $cells.mL^{-1}$ with fresh media. Growth was evaluated using a Malassez cell counting chamber or by the absorption at 730 nm (A_{730}) using a TECAN plate reader.

Automated high-throughput screening

The screening of small molecules was performed using the automated multi-module platform from the CMBA (Centre de criblage pour des molecules bio-actives), Grenoble. An 800 mL-culture of PtYFP was grown in ESAW 1N1P medium, until cell concentration reached $2.5.10^6$

cells.mL^{-1}. Cells were centrifuged at 3,500 rpm for 5 minutes and the supernatant was gently discarded. Cells were then resuspended in a fresh ESAW 0N1P (without nitrogen and containing 2.2.10^{-2} mM NaH_3PO_4) and adjusted to a final concentration of 10^6 cells.mL^{-1}. Clear 48-well plates (NUNC, 055431) were prepared by adding a 4-mm glass bead (Roth, HH55.1) in each well. Firstly, 450 µL aliquots of PtYFP cells were dispensed into the wells corresponding to "high TAG controls", completed with 50 µL of 0N1P medium (cells incubated in 500 µL low-nitrogen medium). $NaNO_3$ was then added to the remaining PtYFP cell suspension (1.0x10^6 cells.mL^{-1}) and mixed gently to obtain a nitrogen-rich medium (ESAW 1N1P, containing 0.55 mM $NaNO_3$ and 2.2x10^{-2} mM NaH_3PO_4). Compounds from the Prestwick Chemical Library were then added in each well, to reach final incubation conditions of 10 µM of compounds, 0.5% DMSO and 1x10^6 cells.mL^{-1}. Glass beads aided culture growth in the 48 well plates. The cultures were incubated for 48 hours at 100 rpm, under a 12 hour / 12 hour - light (50 µmol photons m^{-2} s^{-1}) / dark cycle, at 20°C, in an artificial climate incubator (HT multitron, Infors, Switzerland). Control conditions included therefore cells in ESAW 1N1P ("low TAG controls") and 0N1P ("high TAG controls") grown without any added molecule. After 48 hours, 150 µL were transferred from the 48-well plate to a black 96-well plate (Greiner, 655086), and YFP and chlorophyll fluorescence levels were measured at excitation/emission wavelengths of 515 nm/530 nm, and 440 nm/680 nm, respectively using a TECAN Infinite M1000 plate reader. To assess the accumulation of neutral lipids, 40 µL of Nile Red (2.5 µg.mL^{-1} 9-diethylamino-5-benzo[α]phenoxazinone in DMSO) were added per well, and incubated for 20 minutes at room temperature. Nile Red fluorescence was measured at excitation / emission wavelengths of 530 nm / 580 nm. Compounds triggering an increase in Nile Red fluorescence levels were selected for a secondary screen, with priority given to hit molecules triggering both high Nile Red and high YFP fluorescence. A list of 160 hit molecules were re-evaluated at 10 µM, and based on the obtained results, and then 40 compounds were selected for a tertiary screen.

Dose Response Assays

A double-strength concentration range of selected compounds was obtained by dilution in ESAW 1N1P medium, 1% DMSO, and 250 µL were dispensed in triplicate in 48 well plates (NUNC, 055431). The same volume (250 µL) of a *P. tricornutum* culture at a cell concentration of 2x10^6 cells.mL^{-1} was added in each well, to reach a final condition of 1x10^6 cell.mL^{-1} and 0.5% DMSO in ESAW medium. A 4-mm glass bead (Roth, HH55.1) was added in each well to aid culture growth in the 48 well plates. Plates were then incubated for 48 hours at 100 rpm,

under a 12 hour / 12 hour - light (50 µmol photons m^{-2} s^{-1}) / dark cycle, at 20°C, in an artificial climate incubator (HT multitron, Infors, Switzerland). Control conditions included untreated cells with 0.5 % DMSO, and cells in ESAW medium without $NaNO_3$. After 48 hours, 300 µL was transferred from the 48 well plate to a clear 96 well plate (NUNC, 55260). The absorbance at 730 nm (A_{730}) was measured using a TECAN M1000 plate reader. The concentration of each culture was calculated using the linear relationship between cells.mL^{-1} counting assessed with a Malassez chamber and A_{730}. A 160-µL aliquot was transferred to a black 96-well plate (Greiner, 655086), and chlorophyll fluorescence was measured at excitation and emission wavelengths of 440 nm and 680 nm, respectively. 40 µL of Nile Red (2.5 µg.mL^{-1} in DMSO) was added in each well, and cells were incubated for 20 minutes at room temperature. Nile Red fluorescence was measured at excitation and emission wavelengths of 530 nm and 580 nm, respectively. The relative fluorescence of Nile Red and Chlorophyll were normalized per million cells, and compared as a percentage of the untreated control. The volume of culture remaining in the NUNC clear 96-well plates (140 µL) was used to measure Photosystem II efficiency, represented by the *Fv/Fm* value.

Time Course Assays

Series of flasks containing 20 mL of *P. tricornutum* cells were cultured in parallel for up to 7 days at 100 rpm, under 12 hour / 12 hour - light (50 µmol photons m^{-2} s^{-1}) / dark cycle, at 20°C, in an artificial climate incubator (HT multitron, Infors, Switzerland). Compounds were added at indicated concentrations (0.5% DMSO, final). Each day, aliquots were removed and TAG accumulation was evaluated using Nile Red staining.

Photosynthetic parameters (Fv/Fm)

To determine photosynthesis parameters in cell cultures, room temperature fast chlorophyll fluorescence kinetics were measured using a Speedzen MX fluorescence imaging system (JBeamBio) with settings previously described (Johnson et al., 2009; Allorent et al., 2013). To this end, a 140 µL volume of *P. tricornutum* culture was transferred to a transparent 96 well-plate and dark-incubated for 15-30 min before measurements. Excitation was performed in the blue range (λ = 450 nm, *F0*). *F0* is the steady state fluorescence in dark-adapted cultures, *Fm* is the maximal fluorescence after a saturating light pulse with green light (520 nm) of dark-adapted cultures, *Fm'* the same in light adapted cultures, *Fv* is the difference between *Fm* and *F0*. With these parameters, the maximum efficiency of energy conversion of photosystem II (PSII) can be calculated as *Fv/Fm* (Butler and Kitajima, 1975; Misra et al., 2012).

Glycerolipid analyses

For lipid analysis, *Phaedoctylum* Pt1 cultures were initiated at a $1x10^6$ cells.mL^{-1} concentration and incubated at 20°C, 100 rpm, under a 12 hour / 12 hour - light (50 µmol photons m^{-2} s^{-1}) / dark cycle. Depending on the treatment, cells were collected at day 2, 4 or 7 in 50 mL falcon tubes *via* centrifugation at 3,500 rpm for 10 minutes. Pellets were immediately snap frozen by transfer in liquid nitrogen and stored at -80°C until lipid extraction. After freeze-drying, pellets were suspended in 4 mL of boiling ethanol for 5 minutes to prevent lipid degradation and lipids were extracted as described earlier (Abida et al., 2015) by addition of 2 mL methanol and 8 mL chloroform at room temperature. The mixture was then saturated with argon and stirred for 1 hour at room temperature. After filtration through glass wool, cell remains were rinsed with 3 mL chloroform/methanol 2:1, v/v and 5 mL of NaCl 1% were then added to the filtrate to initiate biphase formation. The chloroform phase was dried under argon before solubilizing the lipid extract in pure chloroform. Total glycerolipids were quantified from their fatty acids: in an aliquot fraction, a known quantity of 15:0 was added and the fatty acids present were transformed as methyl esters (FAME) by a 1-hour incubation in 3 mL 2.5% H_2SO_4 in pure methanol at 100°C. The reaction was stopped by addition of 3 mL water and 3 mL hexane. The hexane phase was analyzed by gas chromatography-flame ionization detector (GC-FID) (Perkin Elmer) on a BPX70 (SGE) column. FAME were identified by comparison of their retention times with those of standards (Sigma) and quantified by the surface peak method using 15:0 for calibration. To quantify the various classes of neutral and polar glycerolipids, lipids were separated by thin layer chromatography (TLC) onto glass-backed silica gel plates (Merck) using two distinct resolving systems. To isolate neutral lipids including TAG and free fatty acid (FFA), lipids were resolved by TLC run in one dimension with hexane:diethylether:acetic acid (70:30:1, v/v). To isolate membrane glycerolipids, lipids were resolved by two-dimensional TLC. The first solvent was chloroform:methanol:water (65:25:4, v/v) and the second one chloroform:acetone:methanol:acetic acid:water (50:20:10:10:5, v/v). Lipids were then visualized under UV light, after spraying with 2% 8-anilino-1-naphthalenesulfonic acid in methanol, and scraped off the plate. FAMEs, were then prepared by methanolysis directly from the silica and quantified by GC-FID as described above.

Screening statistics.

Quality of screening assay was assessed based on the calculation of the *Z'* factor (Zhang et al., 1999), with the following equation:

$$Z' = 1 - (3\sigma_{c+} + 3\sigma_{c-})/|\mu_{c+} - \mu_{c-}|$$

with σ_{c+} and σ_{c-} the standard deviation of readout values obtained with positive and negative controls, and μ_{c+} and μ_{c-} the means of readout values obtained with positive and negative controls *i.e.* high-TAG and low-TAG controls respectively.

Transcriptomic analyses

Phaeodactylum cells were grown in 50 mL of ESAW medium in 100-mL flasks, until they reached a minimum concentration of 6.10^6 cells.mL^{-1}. Cells were then incubated 4 days with increasing concentrations of 17α-Ethynylestradiol, provided at 0, 10 and 20 µM, with a final concentration of DMSO 0.5%. Following treatment, frozen cells (2.10^8 cells) were sent to BGI (Hongkong, China) for RNA extraction using the TRIzol reagent (Chomczynski and Sacchi, 1987) allowing the collection of 10-20 µg RNA per sample. Quality was assessed based on the 28S/18S ratio and RNA Integrity Number (RIN) tests, using an Agilent 2100 Bioanalyzer. Libraries were prepared for stranded 100 bp paired end sequencing and samples were analyzed independently using an Illumina Hiseq 4000 system (20 M reads). Reads were mapped on the most recent genome version of *Phaeodactylum tricornutum* (http://protists.ensembl.org/Phaeodactylum_tricornutum/Info/Index) using the Star (Spliced Transcripts Alignment to a Reference) method (Dobin et al., 2013; Engstrom et al., 2013). Data were filtered based on the detection of 1 read in at least one sample per treatment or genomic mutation and then normalized using the DESseq2 method (Varet et al., 2016). Clustering was achieved based on expression profiles as described previously (Dolch et al., 2017).

Accession numbers

Sequences from the *Phaedoactylum* genome analyzed more carefully in the present study can be found *via* Ensembl! under the following accession numbers: Phatr3_EG01524; Phatr3_EG01947; Phatr3_EG01955; Phatr3_EG02208; Phatr3_EG02286; Phatr3_EG02309; Phatr3_EG02454; Phatr3_EG02496; Phatr3_EG02521; Phatr3_EG02619; Phatr3_J10068; Phatr3_J10497; Phatr3_J11319; Phatr3_J11390; Phatr3_J11811; Phatr3_J11916; Phatr3_J12420; Phatr3_J12420; Phatr3_J12431; Phatr3_J12642; Phatr3_J12740; Phatr3_J12884; Phatr3_J12902; Phatr3_J13073; Phatr3_J13076; Phatr3_J14202; Phatr3_J15031; Phatr3_J15211; Phatr3_J15730; Phatr3_J16364; Phatr3_J16376; Phatr3_J17086; Phatr3_J17720; Phatr3_J17720; Phatr3_J18029; Phatr3_J18064; Phatr3_J18940; Phatr3_J18940; Phatr3_J1971; Phatr3_J19979; Phatr3_J20143;

Phatr3_J20143; Phatr3_J20310; Phatr3_J20342; Phatr3_J20460; Phatr3_J20460; Phatr3_J20508; Phatr3_J21116; Phatr3_J21201; Phatr3_J21988; Phatr3_J22122; Phatr3_J2215; Phatr3_J22274; Phatr3_J22357; Phatr3_J22404; Phatr3_J22459; Phatr3_J22510; Phatr3_J22554; Phatr3_J22677; Phatr3_J22803; Phatr3_J23639; Phatr3_J23850; Phatr3_J23913; Phatr3_J24195; Phatr3_J24610; Phatr3_J24739; Phatr3_J25769; Phatr3_J25932; Phatr3_J26029; Phatr3_J26714; Phatr3_J28009; Phatr3_J28068; Phatr3_J28652; Phatr3_J28797; Phatr3_J29157; Phatr3_J29488; Phatr3_J29702; Phatr3_J30113; Phatr3_J30145; Phatr3_J30282; Phatr3_J30514; Phatr3_J31367; Phatr3_J31440; Phatr3_J31492; Phatr3_J31662; Phatr3_J31994; Phatr3_J31994; Phatr3_J32083; Phatr3_J3262; Phatr3_J32902; Phatr3_J33198; Phatr3_J33435; Phatr3_J33720; Phatr3_J33864; Phatr3_J33864; Phatr3_J34485; Phatr3_J34526; Phatr3_J35240; Phatr3_J36821; Phatr3_J37086; Phatr3_J37086; Phatr3_J37367; Phatr3_J37372; Phatr3_J37652; Phatr3_J38509; Phatr3_J39710; Phatr3_J39949; Phatr3_J40163; Phatr3_J40200; Phatr3_J40261; Phatr3_J40880; Phatr3_J40988; Phatr3_J41423; Phatr3_J41423; Phatr3_J41515; Phatr3_J41570; Phatr3_J41886; Phatr3_J41969; Phatr3_J42398; Phatr3_J42683; Phatr3_J42872; Phatr3_J43010; Phatr3_J43099; Phatr3_J43116; Phatr3_J43320; Phatr3_J43352; Phatr3_J43463; Phatr3_J43469; Phatr3_J43678; Phatr3_J43773; Phatr3_J43773; Phatr3_J43773; Phatr3_J44005; Phatr3_J44028; Phatr3_J44066; Phatr3_J44231; Phatr3_J44401; Phatr3_J44584; Phatr3_J44645; Phatr3_J44806; Phatr3_J44831; Phatr3_J45223; Phatr3_J45510; Phatr3_J45510; Phatr3_J45518; Phatr3_J45551; Phatr3_J45758; Phatr3_J45947; Phatr3_J46175; Phatr3_J46453; Phatr3_J46570; Phatr3_J46595; Phatr3_J46830; Phatr3_J47389; Phatr3_J48423; Phatr3_J48664; Phatr3_J48778; Phatr3_J48778; Phatr3_J48799; Phatr3_J48859; Phatr3_J48977; Phatr3_J49163; Phatr3_J4918; Phatr3_J49339; Phatr3_J49462; Phatr3_J49524; Phatr3_J49544; Phatr3_J49771; Phatr3_J49867; Phatr3_J50356; Phatr3_J50742; Phatr3_J50770; Phatr3_J51214; Phatr3_J51454; Phatr3_J51519; Phatr3_J52268; Phatr3_J52368; Phatr3_J52648; Phatr3_J5271; Phatr3_J54017; Phatr3_J54068; Phatr3_J54151; Phatr3_J54168; Phatr3_J54222; Phatr3_J54494; Phatr3_J54528; Phatr3_J54709; Phatr3_J54709; Phatr3_J54974; Phatr3_J54983; Phatr3_J55069; Phatr3_J55111; Phatr3_J55153; Phatr3_J55157; Phatr3_J55192; Phatr3_J55209; Phatr3_J5527; Phatr3_J7164; Phatr3_J7678; Phatr3_J8663; Phatr3_J8860; Phatr3_J8975; Phatr3_J9255; Phatr3_J9316; Phatr3_J9538; Phatr3_J9619; Phatr3_J9709; Phatr3_J9794; Phatr3_Jdraft559; Phatr3_J23913; Phatr3_J1664 ; Phatr3_J16870; Phatr3_J53929;

Phatr3_EG02641; Phatr3_EG02359; Phatr3_EG00741; Phatr3_J12533; Phatr3_EG02290; Phatr3_J47271; Phatr3_J49325; Phatr3_EG02293; Phatr3_J10824; Phatr3_J49447; Phatr3_J31339; Phatr3_J10852; Phatr3_J48864; Phatr3_J36801; Phatr3_J14208; Phatr3_J30461; Phatr3_J51757; Phatr3_J1689; Phatr3_J9258; Phatr3_J12330; Phatr3_EG02383; Phatr3_J12330; Phatr3_J44955; Phatr3_J41845.

Acknowledgements

This work was supported by grants from Agence Nationale de la Recherche (ANR DiaDomOil), CEA (Irtelis and Flagship PhD grant programs), Programme Investissement d'Avenir (Océanomics). Authors are grateful to Séverine Collin, Marie-Odile Fauvarque, Michel Ferrand, Giovanni Finazzi and Dimitris Petroutsos for fruitful discussions and advices.

References.

Abida H, Dolch LJ, Mei C, Villanova V, Conte M, Block MA, Finazzi G, Bastien O, Tirichine L, Bowler C, Rebeille F, Petroutsos D, Jouhet J, Marechal E (2015) Membrane glycerolipid remodeling triggered by nitrogen and phosphorus starvation in Phaeodactylum tricornutum. Plant Physiol **167:** 118-136

Adeel M, Song X, Wang Y, Francis D, Yang Y (2017) Environmental impact of estrogens on human, animal and plant life: A critical review. Environ Int **99:** 107-119

Ajjawi I, Verruto J, Aqui M, Soriaga LB, Coppersmith J, Kwok K, Peach L, Orchard E, Kalb R, Xu WD, Carlson TJ, Francis K, Konigsfeld K, Bartalis J, Schultz A, Lambert W, Schwartz AS, Brown R, Moellering ER (2017) Lipid production in Nannochloropsis gaditana is doubled by decreasing expression of a single transcriptional regulator. Nature Biotechnology **35:** 647-+

Alipanah L, Rohloff J, Winge P, Bones AM, Brembu T (2015) Whole-cell response to nitrogen deprivation in the diatom Phaeodactylum tricornutum. J Exp Bot **66:** 6281-6296

Allorent G, Courtois F, Chevalier F, Lerbs-Mache S (2013) Plastid gene expression during chloroplast differentiation and dedifferentiation into non-photosynthetic plastids during seed formation. Plant Mol Biol **82:** 59-70

Anandarajah K, Mahendraperumal G, Sommerfeld M, Hu Q (2012) Characterization of microalga Nannochloropsis sp mutants for improved production of biofuels. Applied Energy **96:** 371-377

Arbenz A, Perrin R, Avérous L (2017) Elaboration and properties of innovative biobased PUIR Foams from microalgae. J Polym Environ**:** In press

Aris AZ, Shamsuddin AS, Praveena SM (2014) Occurrence of 17alpha-ethynylestradiol (EE2) in the environment and effect on exposed biota: a review. Environ Int **69:** 104-119

Armbrust EV, Berges JA, Bowler C, Green BR, Martinez D, Putnam NH, Zhou S, Allen AE, Apt KE, Bechner M, Brzezinski MA, Chaal BK, Chiovitti A, Davis AK, Demarest MS, Detter JC, Glavina T, Goodstein D, Hadi MZ, Hellsten U, Hildebrand M, Jenkins BD, Jurka J, Kapitonov VV, Kroger N, Lau WW, Lane TW, Larimer FW, Lippmeier JC, Lucas S, Medina M, Montsant A, Obornik M, Parker MS, Palenik B, Pazour GJ, Richardson PM, Rynearson TA, Saito MA, Schwartz DC, Thamatrakoln K, Valentin K, Vardi A, Wilkerson FP, Rokhsar DS (2004) The genome of the diatom Thalassiosira pseudonana: ecology, evolution, and metabolism. Science **306:** 79-86

Attwood D (1976) Aggregation of antiacetylcholine drugs in aqueous solution: micellar properties of some diphenylmethane derivatives. J Pharm Pharmacol **28:** 407-409

Baas PW, Rao AN, Matamoros AJ, Leo L (2016) Stability properties of neuronal microtubules. Cytoskeleton (Hoboken) **73:** 442-460

Bergstrom JD, Bostedor RG, Masarachia PJ, Reszka AA, Rodan G (2000) Alendronate is a specific, nanomolar inhibitor of farnesyl diphosphate synthase. Arch Biochem Biophys **373:** 231-241

Bhandari RK, Deem SL, Holliday DK, Jandegian CM, Kassotis CD, Nagel SC, Tillitt DE, Vom Saal FS, Rosenfeld CS (2015) Effects of the environmental estrogenic contaminants bisphenol A and 17alpha-ethinyl estradiol on sexual development and adult behaviors in aquatic wildlife species. Gen Comp Endocrinol **214:** 195-219

Blagosklonny MV (2003) A new science-business paradigm in anticancer drug development. Trends in Biotechnology **21:** 103-106

Botte CY, Marechal E (2014) Plastids with or without galactoglycerolipids. Trends Plant Sci **19:** 71-78

Bowler C, Allen AE, Badger JH, Grimwood J, Jabbari K, Kuo A, Maheswari U, Martens C, Maumus F, Otillar RP, Rayko E, Salamov A, Vandepoele K, Beszteri B, Gruber A, Heijde M, Katinka M, Mock T, Valentin K, Verret F, Berges JA, Brownlee C, Cadoret JP, Chiovitti A, Choi CJ, Coesel S, De Martino A, Detter JC, Durkin C, Falciatore A, Fournet J, Haruta M, Huysman MJ, Jenkins BD, Jiroutova K, Jorgensen RE, Joubert Y, Kaplan A, Kroger N, Kroth PG, La Roche J, Lindquist E, Lommer M, Martin-Jezequel V, Lopez PJ, Lucas S, Mangogna M, McGinnis K, Medlin LK, Montsant A, Oudot-Le Secq MP, Napoli C, Obornik M, Parker MS, Petit JL, Porcel BM, Poulsen N, Robison M, Rychlewski L, Rynearson TA, Schmutz J, Shapiro H, Siaut M, Stanley M, Sussman MR, Taylor AR, Vardi A, von Dassow P, Vyverman W, Willis A, Wyrwicz LS, Rokhsar DS, Weissenbach J, Armbrust EV, Green BR, Van de Peer Y, Grigoriev IV (2008) The Phaeodactylum genome reveals the evolutionary history of diatom genomes. Nature **456:** 239-244

Bozarth A, Maier UG, Zauner S (2009) Diatoms in biotechnology: modern tools and applications. Appl Microbiol Biotechnol **82:** 195-201

Brodie J, Chan CX, De Clerck O, Cock JM, Coelho SM, Gachon C, Grossman AR, Mock T, Raven JA, Smith AG, Yoon HS, Bhattacharya D (2017) The Algal Revolution. Trends Plant Sci **22:** 726-738

Butler WL, Kitajima M (1975) Fluorescence quenching in photosystem II of chloroplasts. Biochim Biophys Acta **376:** 116-125

Camell CD, Sander J, Spadaro O, Lee A, Nguyen KY, Wing A, Goldberg EL, Youm YH, Brown CW, Elsworth J, Rodeheffer MS, Schultze JL, Dixit VD (2017) Inflammasome-driven catecholamine catabolism in macrophages blunts lipolysis during ageing. Nature **550:** 119-123

Chen CS, Jounaidi Y, Waxman DJ (2005) Enantioselective metabolism and cytotoxicity of R-ifosfamide and S-ifosfamide by tumor cell-expressed cytochromes P450. Drug Metab Dispos **33:** 1261-1267

Chen X, Ji ZL, Chen YZ (2002) TTD: Therapeutic Target Database. Nucleic Acids Res **30:** 412-415

Chesne C, Guyomard C, Guillouzo A, Schmid J, Ludwig E, Sauter T (1998) Metabolism of Meloxicam in human liver involves cytochromes P4502C9 and 3A4. Xenobiotica **28:** 1-13

Chisti Y (2013) Constraints to commercialization of algal fuels. J Biotechnol **167:** 201-214

Chomczynski P, Sacchi N (1987) Single-step method of RNA isolation by acid guanidinium thiocyanate-phenol-chloroform extraction. Anal Biochem **162:** 156-159

Coelho AM, Jacob L, Fioramonti J, Bueno L (2001) Rectal antinociceptive properties of alverine citrate are linked to antagonism at the 5-HT1A receptor subtype. J Pharm Pharmacol **53:** 1419-1426

Coleman DT, Gray AL, Stephens CA, Scott ML, Cardelli JA (2016) Repurposed drug screen identifies cardiac glycosides as inhibitors of TGF-beta-induced cancer-associated fibroblast differentiation. Oncotarget **7:** 32200-32209

Corteggiani Carpinelli E, Telatin A, Vitulo N, Forcato C, D'Angelo M, Schiavon R, Vezzi A, Giacometti GM, Morosinotto T, Valle G (2014) Chromosome scale genome assembly and transcriptome profiling of Nannochloropsis gaditana in nitrogen depletion. Mol Plant **7:** 323-335

Cvejic JH, Rohmer M (2000) CO2 as main carbon source for isoprenoid biosynthesis via the mevalonate-independent methylerythritol 4-phosphate route in the marine diatoms Phaeodactylum tricornutum and Nitzschia ovalis. Phytochemistry **53:** 21-28

d'Ippolito G, Sardo A, Paris D, Vella FM, Adelfi MG, Botte P, Gallo C, Fontana A (2015) Potential of lipid metabolism in marine diatoms for biofuel production. Biotechnol Biofuels **8:** 28

Daboussi F, Leduc S, Marechal A, Dubois G, Guyot V, Perez-Michaut C, Amato A, Falciatore A, Juillerat A, Beurdeley M, Voytas DF, Cavarec L, Duchateau P (2014) Genome engineering empowers the diatom Phaeodactylum tricornutum for biotechnology. Nat Commun **5:** 3831

De Riso V, Raniello R, Maumus F, Rogato A, Bowler C, Falciatore A (2009) Gene silencing in the marine diatom Phaeodactylum tricornutum. Nucleic Acids Res **37:** e96

Deschamps P, Moreira D (2012) Reevaluating the green contribution to diatom genomes. Genome Biol Evol **4:** 683-688

Dobin A, Davis CA, Schlesinger F, Drenkow J, Zaleski C, Jha S, Batut P, Chaisson M, Gingeras TR (2013) STAR: ultrafast universal RNA-seq aligner. Bioinformatics **29:** 15-21

Dolch LJ, Lupette J, Tourcier G, Bedhomme M, Collin S, Magneschi L, Conte M, Seddiki K, Richard C, Corre E, Fourage L, Laeuffer F, Richards R, Reith M, Rebeille F, Jouhet J, McGinn P, Marechal E (2017) NO mediates nitrite-sensing and adaptation and triggers a remodeling of lipids. Plant Physiol

Dolch LJ, Marechal E (2015) Inventory of fatty acid desaturases in the pennate diatom Phaeodactylum tricornutum. Mar Drugs **13:** 1317-1339

Dolch LJ, Rak C, Perin G, Tourcier G, Broughton R, Leterrier M, Morosinotto T, Tellier F, Faure JD, Falconet D, Jouhet J, Sayanova O, Beaudoin F, Marechal E (2017) A Palmitic Acid Elongase Affects Eicosapentaenoic Acid and Plastidial Monogalactosyldiacylglycerol Levels in Nannochloropsis. Plant Physiol **173:** 742-759

Engstrom PG, Steijger T, Sipos B, Grant GR, Kahles A, Ratsch G, Goldman N, Hubbard TJ, Harrow J, Guigo R, Bertone P, Consortium R (2013) Systematic evaluation of spliced alignment programs for RNA-seq data. Nat Methods **10:** 1185-1191

Fabris M, Matthijs M, Carbonelle S, Moses T, Pollier J, Dasseville R, Baart GJ, Vyverman W, Goossens A (2014) Tracking the sterol biosynthesis pathway of the diatom Phaeodactylum tricornutum. New Phytol **204:** 521-535

Falciatore A, Casotti R, Leblanc C, Abrescia C, Bowler C (1999) Transformation of Nonselectable Reporter Genes in Marine Diatoms. Mar Biotechnol (NY) **1:** 239-251

Falciatore A, d'Alcala MR, Croot P, Bowler C (2000) Perception of environmental signals by a marine diatom. Science **288:** 2363-2366

Flori S, Jouneau PH, Finazzi G, Marechal E, Falconet D (2016) Ultrastructure of the Periplastidial Compartment of the Diatom Phaeodactylum tricornutum. Protist **167:** 254-267

Francis SH, Busch JL, Corbin JD, Sibley D (2010) cGMP-dependent protein kinases and cGMP phosphodiesterases in nitric oxide and cGMP action. Pharmacol Rev **62:** 525-563

Franz AK, Danielewicz MA, Wong DM, Anderson LA, Boothe JR (2013) Phenotypic screening with oleaginous microalgae reveals modulators of lipid productivity. ACS Chem Biol **8:** 1053-1062

Fukaya N, Mochizuki K, Tanaka Y, Kumazawa T, Jiuxin Z, Fuchigami M, Goda T (2009) The alpha-glucosidase inhibitor miglitol delays the development of diabetes and dysfunctional insulin secretion in pancreatic beta-cells in OLETF rats. Eur J Pharmacol **624:** 51-57

Furlanut M, Franceschi L (2003) Pharmacology of ifosfamide. Oncology **65 Suppl 2:** 2-6

Gallo C, d'Ippolito G, Nuzzo G, Sardo A, Fontana A (2017) Autoinhibitory sterol sulfates mediate programmed cell death in a bloom-forming marine diatom. Nat Commun **8:** 1292

Gardner MJ, Hall N, Fung E, White O, Berriman M, Hyman RW, Carlton JM, Pain A, Nelson KE, Bowman S, Paulsen IT, James K, Eisen JA, Rutherford K, Salzberg SL, Craig A, Kyes S, Chan MS, Nene V, Shallom SJ, Suh B, Peterson J, Angiuoli S, Pertea M, Allen J, Selengut J, Haft D, Mather MW, Vaidya AB, Martin DM, Fairlamb AH, Fraunholz MJ, Roos DS, Ralph SA, McFadden GI, Cummings LM, Subramanian GM, Mungall C, Venter JC, Carucci DJ, Hoffman SL, Newbold C, Davis RW, Fraser CM, Barrell B (2002) Genome sequence of the human malaria parasite Plasmodium falciparum. Nature **419:** 498-511

Georgakopoulos ND, Wells G, Campanella M (2017) The pharmacological regulation of cellular mitophagy. Nat Chem Biol **13:** 136-146

Gould SB, Waller RF, McFadden GI (2008) Plastid evolution. Annu Rev Plant Biol **59:** 491-517

Haenisch B, Walstab J, Herberhold S, Bootz F, Tschaikin M, Ramseger R, Bonisch H (2010) Alpha-adrenoceptor agonistic activity of oxymetazoline and xylometazoline. Fundam Clin Pharmacol **24:** 729-739

Haggarty SJ, Mayer TU, Miyamoto DT, Fathi R, King RW, Mitchison TJ, Schreiber SL (2000) Dissecting cellular processes using small molecules: identification of colchicine-like, taxol-like and other small molecules that perturb mitosis. Chem Biol **7:** 275-286

Haraguchi K, Ito K, Kotaki H, Sawada Y, Iga T (1997) Prediction of drug-induced catalepsy based on dopamine D1, D2, and muscarinic acetylcholine receptor occupancies. Drug Metab Dispos **25:** 675-684

Huang XP, Williams FE, Peseckis SM, Messer WS, Jr. (1998) Pharmacological characterization of human m1 muscarinic acetylcholine receptors with double mutations at the junction of TM VI and the third extracellular domain. J Pharmacol Exp Ther **286:** 1129-1139

Imming P, Sinning C, Meyer A (2006) Drugs, their targets and the nature and number of drug targets. Nat Rev Drug Discov **5:** 821-834

Inhoffen HH, Hohlweg W (1938) Neue per os-wirksame weibliche Keimdrüsenhormon-Derivate: 17-Aethinyl-oestradiol und Pregnen-in-on-3-ol-17. Naturwissenschaften **26:** 96

Jensen EV, DeSombre ER (1973) Estrogen-receptor interaction. Science **182:** 126-134

Jeong DE, Song HJ, Lim S, Lee SJ, Lim JE, Nam DH, Joo KM, Jeong BC, Jeon SS, Choi HY, Lee HW (2015) Repurposing the anti-malarial drug artesunate as a novel therapeutic agent for metastatic renal cell carcinoma due to its attenuation of tumor growth, metastasis, and angiogenesis. Oncotarget **6:** 33046-33064

Johnson X, Vandystadt G, Bujaldon S, Wollman FA, Dubois R, Roussel P, Alric J, Beal D (2009) A new setup for in vivo fluorescence imaging of photosynthetic activity. Photosynth Res **102:** 85-93

Keeling PJ (2009) Chromalveolates and the evolution of plastids by secondary endosymbiosis. J Eukaryot Microbiol **56:** 1-8

Kilian O, Benemann CS, Niyogi KK, Vick B (2011) High-efficiency homologous recombination in the oil-producing alga Nannochloropsis sp. Proc Natl Acad Sci U S A **108:** 21265-21269

Kim J, Brown CM, Kim MK, Burrows EH, Bach S, Lun DS, Falkowski PG (2017) Effect of cell cycle arrest on intermediate metabolism in the marine diatom Phaeodactylum tricornutum. Proc Natl Acad Sci U S A **114:** E8007-E8016

Klein-Marcuschamer D, Chisti Y, Benemann JR, Lewis D (2013) A matter of detail: assessing the true potential of microalgal biofuels. Biotechnol Bioeng **110:** 2317-2322

Kutschera U, Niklas KJ (2005) Endosymbiosis, cell evolution, and speciation. Theory in Biosciences **124:** 1-24

Larsen M, Holm R, Jensen KG, Sveigaard C, Brodin B, Nielsen CU (2010) 5-Hydroxy-L-tryptophan alters gaboxadol pharmacokinetics in rats: involvement of PAT1 and rOat1 in gaboxadol absorption and elimination. Eur J Pharm Sci **39:** 68-75

Levitan O, Dinamarca J, Hochman G, Falkowski PG (2014) Diatoms: a fossil fuel of the future. Trends Biotechnol **32:** 117-124

Levitan O, Dinamarca J, Zelzion E, Lun DS, Guerra LT, Kim MK, Kim J, Van Mooy BA, Bhattacharya D, Falkowski PG (2015) Remodeling of intermediate metabolism in the diatom Phaeodactylum tricornutum under nitrogen stress. Proc Natl Acad Sci U S A **112:** 412-417

Liao JC, Mi L, Pontrelli S, Luo S (2016) Fuelling the future: microbial engineering for the production of sustainable biofuels. Nat Rev Microbiol **14:** 288-304

Lipinski CA, Lombardo F, Dominy BW, Feeney PJ (2001) Experimental and computational approaches to estimate solubility and permeability in drug discovery and development settings. Adv Drug Deliv Rev **46:** 3-26

Liu L, Zhang R, Zhao JJ, Rogers JD, Hsieh JY, Fang W, Matuszewski BK, Dobrinska MR (2003) Determination of simvastatin-derived HMG-CoA reductase inhibitors in biomatrices using an automated enzyme inhibition assay with radioactivity detection. J Pharm Biomed Anal **32:** 107-123

Liu T, Zhang S, Chen J, Jiang K, Zhang Q, Guo K, Liu Y (2014) The transcriptional profiling of glycogenes associated with hepatocellular carcinoma metastasis. PLoS One **9:** e107941

Liu Y, Guan Y, Gao Q, Tam NF, Zhu W (2010) Cellular responses, biodegradation and bioaccumulation of endocrine disrupting chemicals in marine diatom Navicula incerta. Chemosphere **80:** 592-599

Liu Y, Tam NFY, Guan YT, Gao BY (2012) Influence of a Marine Diatom on the Embryonic Toxicity of 17 alpha-Ethynylestradiol to the Abalone Haliotis diversicolor supertexta. Water Air and Soil Pollution **223:** 4383-4395

Lupette J, Maréchal E (2018) Phytoplankton glycerolipids, challenging but promising prospects from biomedicine to green chemistry and biofuels. *In* S La Barre, SS Bates, eds, Blue Technologies: production and use of marine molecules. Wiley VCH, Weinheim, Germany, , p In press

Maeda Y, Nojima D, Yoshino T, Tanaka T (2017) Structure and properties of oil bodies in diatoms. Philos Trans R Soc Lond B Biol Sci **372:** 20160408

Maier UG, Douglas SE, Cavalier-Smith T (2000) The nucleo morph genomes of cryptophytes and chlorarachniophytes. Protist **151:** 103-109

Mainardi JL, Villet R, Bugg TD, Mayer C, Arthur M (2008) Evolution of peptidoglycan biosynthesis under the selective pressure of antibiotics in Gram-positive bacteria. FEMS Microbiol Rev **32:** 386-408

Marechal E (2008) Chemogenomics: a discipline at the crossroad of high throughput technologies, biomarker research, combinatorial chemistry, genomics, cheminformatics, bioinformatics and artificial intelligence. Comb Chem High Throughput Screen **11:** 582

Marechal E (2009) In Silico Strategies for Target Discovery. Infection Genetics and Evolution **9:** 370-371

Mayer TU, Kapoor TM, Haggarty SJ, King RW, Schreiber SL, Mitchison TJ (1999) Small molecule inhibitor of mitotic spindle bipolarity identified in a phenotype-based screen. Science **286:** 971-974

McFadden GI (1999) Endosymbiosis and evolution of the plant cell. Curr Opin Plant Biol **2:** 513-519

Meï CE, Cussac M, Haslam RP, Beaudoin F, Wong YS, Marechal E, Rébeillé F (2017) C1 metabolism inhibition and nitrogen deprivation trigger triacylglycerol accumulation in Arabidopsis thaliana cell cultures and highlithgt a role of NPC in phosphatidylcholine-to-triacylglycerol pathway. . Front. Plant Sci.

Merchant SS, Prochnik SE, Vallon O, Harris EH, Karpowicz SJ, Witman GB, Terry A, Salamov A, Fritz-Laylin LK, Marechal-Drouard L, Marshall WF, Qu LH, Nelson DR, Sanderfoot AA, Spalding MH, Kapitonov VV, Ren Q, Ferris P, Lindquist E, Shapiro H, Lucas SM, Grimwood J, Schmutz J, Cardol P, Cerutti H, Chanfreau G, Chen CL, Cognat V, Croft MT, Dent R, Dutcher S, Fernandez E, Fukuzawa H, Gonzalez-Ballester D, Gonzalez-Halphen D, Hallmann A, Hanikenne M, Hippler M, Inwood W, Jabbari K, Kalanon M, Kuras R, Lefebvre PA, Lemaire SD, Lobanov AV, Lohr M, Manuell A, Meier I, Mets L, Mittag M, Mittelmeier T, Moroney JV, Moseley J, Napoli C, Nedelcu AM, Niyogi K, Novoselov SV, Paulsen IT, Pazour G, Purton S, Ral JP, Riano-Pachon DM, Riekhof W, Rymarquis L, Schroda M, Stern D, Umen J, Willows R, Wilson N, Zimmer SL, Allmer J, Balk J, Bisova K, Chen CJ, Elias M, Gendler K, Hauser C, Lamb MR, Ledford H, Long JC, Minagawa J, Page MD, Pan J, Pootakham W, Roje S, Rose A, Stahlberg E, Terauchi AM, Yang P, Ball S, Bowler C, Dieckmann CL, Gladyshev VN, Green P, Jorgensen R, Mayfield S, Mueller-Roeber B, Rajamani S, Sayre RT, Brokstein P, Dubchak I, Goodstein D, Hornick L, Huang YW, Jhaveri J, Luo Y, Martinez D, Ngau WC, Otillar B, Poliakov A, Porter A, Szajkowski L, Werner G, Zhou K, Grigoriev IV, Rokhsar DS, Grossman AR (2007) The Chlamydomonas genome reveals the evolution of key animal and plant functions. Science **318:** 245-250

Misra AN, Misra M, Singh R (2012) Chlorophyll fluorescence in plant biology. *In* AN Misra, ed, Biophysics. InTech, pp 171-192

Nataraj C, Thomas DW, Tilley SL, Nguyen MT, Mannon R, Koller BH, Coffman TM (2001) Receptors for prostaglandin E(2) that regulate cellular immune responses in the mouse. J Clin Invest **108:** 1229-1235

Nymark M, Sharma AK, Sparstad T, Bones AM, Winge P (2016) A CRISPR/Cas9 system adapted for gene editing in marine algae. Sci. Rep. **6:** 24951

Overington JP, Al-Lazikani B, Hopkins AL (2006) How many drug targets are there? Nat Rev Drug Discov **5:** 993-996

Pacher P, Nivorozhkin A, Szabo C (2006) Therapeutic effects of xanthine oxidase inhibitors: renaissance half a century after the discovery of allopurinol. Pharmacol Rev **58:** 87-114

Panara MR, Renda G, Sciulli MG, Santini G, Di Giamberardino M, Rotondo MT, Tacconelli S, Seta F, Patrono C, Patrignani P (1999) Dose-dependent inhibition of platelet cyclooxygenase-1 and monocyte cyclooxygenase-2 by meloxicam in healthy subjects. J Pharmacol Exp Ther **290:** 276-280

Pawlowski L, Siwanowicz J, Bigajska K, Przegalinski E (1985) Central antiserotonergic and antidopaminergic action of pirenperone, a putative 5-HT2 receptor antagonist. Pol J Pharmacol Pharm **37:** 179-196

Petroutsos D, Amiar S, Abida H, Dolch LJ, Bastien O, Rebeille F, Jouhet J, Falconet D, Block MA, McFadden GI, Bowler C, Botte C, Marechal E (2014) Evolution of galactoglycerolipid biosynthetic pathways--from cyanobacteria to primary plastids and from primary to secondary plastids. Prog Lipid Res **54:** 68-85

Pocock T, Falk S (2014) Negative impact on growth and photosynthesis in the green alga Chlamydomonas reinhardtii in the presence of the estrogen 17alpha-ethynylestradiol. PLoS One **9:** e109289

Preissner S, Kroll K, Dunkel M, Senger C, Goldsobel G, Kuzman D, Guenther S, Winnenburg R, Schroeder M, Preissner R (2010) SuperCYP: a comprehensive database on Cytochrome P450 enzymes including a tool for analysis of CYP-drug interactions. Nucleic Acids Res **38:** D237-243

Priddy AR, Killick SR, Elstein M, Morris J, Sullivan M, Patel L, Elder M (1990) The effect of prostaglandin synthetase inhibitors on human preovulatory follicular fluid prostaglandin, thromboxane, and leukotriene concentrations. J Clin Endocrinol Metab **71:** 235-242

Prioretti L, Avilan L, Carriere F, Montane MH, Field B, Gregori G, Menand B, Gontero B (2017) The inhibition of TOR in the model diatom Phaeodactylum tricornutum promotes a get-fat growth regime. Algal Research-Biomass Biofuels and Bioproducts **26:** 265-274

Pulz O, Gross W (2004) Valuable products from biotechnology of microalgae. Appl Microbiol Biotechnol **65:** 635-648

Pytliak M, Vargova V, Mechirova V, Felsoci M (2011) Serotonin receptors - from molecular biology to clinical applications. Physiol Res **60:** 15-25

Qian H, Martin RJ, Robertson AP (2006) Pharmacology of N-, L-, and B-subtypes of nematode nAChR resolved at the single-channel level in Ascaris suum. FASEB J **20:** 2606-2608

Riva E, Mennini T, Latini R (1991) The alpha- and beta-adrenoceptor blocking activities of labetalol and its RR-SR (50:50) stereoisomers. Br J Pharmacol **104:** 823-828

Ruiz J, Olivieri G, de Vree J, Bosma R, Willems P, Reith JH, Eppink MHM, Kleinegris DMM, Wijffels RH, Barbosa MJ (2016) Towards industrial products from microalgae. Energy Environ. Sci. **In press**

Sayanova O, Mimouni V, Ulmann L, Morant-Manceau A, Pasquet V, Schoefs B, Napier JA (2017) Modulation of lipid biosynthesis by stress in diatoms. Philos Trans R Soc Lond B Biol Sci **372**

Sayanova OV, Napier JA (2004) Eicosapentaenoic acid: biosynthetic routes and the potential for synthesis in transgenic plants. Phytochemistry **65:** 147-158

Scaife MA, Smith AG (2016) Towards developing algal synthetic biology. Biochem Soc Trans **44:** 716-722

Schudt C, Winder S, Eltze M, Kilian U, Beume R (1991) Zardaverine: a cyclic AMP specific PDE III/IV inhibitor. Agents Actions Suppl **34:** 379-402

Shikanai T (2014) Central role of cyclic electron transport around photosystem I in the regulation of photosynthesis. Curr Opin Biotechnol **26:** 25-30

Shteinikov VY, Korosteleva AS, Tikhonova TB, Potapieva NN, Tikhonov DB (2017) Ligands of histamine receptors modulate acid-sensing ion channels. Biochem Biophys Res Commun **490:** 1314-1318

Siaut M, Heijde M, Mangogna M, Montsant A, Coesel S, Allen A, Manfredonia A, Falciatore A, Bowler C (2007) Molecular toolbox for studying diatom biology in Phaeodactylum tricornutum. Gene **406:** 23-35

Siegenthaler PF, Bain P, Riva F, Fent K (2017) Effects of antiandrogenic progestins, chlormadinone and cyproterone acetate, and the estrogen 17alpha-ethinylestradiol (EE2), and their mixtures: Transactivation with human and rainbowfish hormone receptors and transcriptional effects in zebrafish (Danio rerio) eleuthero-embryos. Aquat Toxicol **182:** 142-162

Soleilhac E, Nadon R, Lafanechere L (2010) High-content screening for the discovery of pharmacological compounds: advantages, challenges and potential benefits of recent technological developments. Expert Opin Drug Discov **5:** 135-144

Somuncu S, Cakmak M, Erdogan S, Caglayan O, Akman H, Kaya M (2005) Trapidil, an inhibitor for phosphodiesterase and platelet-derived-growth factor, ameliorates corrosive esophageal burn in rats. Tohoku J Exp Med **207:** 203-208

Spolaore P, Joannis-Cassan C, Duran E, Isambert A (2006) Commercial applications of microalgae. J Biosci Bioeng **101:** 87-96

Stoebe B, Maier UG (2002) One, two, three: nature's tool box for building plastids. Protoplasma **219:** 123-130

Tornio A, Pasanen MK, Laitila J, Neuvonen PJ, Backman JT (2005) Comparison of 3-hydroxy-3-methylglutaryl coenzyme A (HMG-CoA) reductase inhibitors (statins) as inhibitors of cytochrome P450 2C8. Basic Clin Pharmacol Toxicol **97:** 104-108

Totir MA, Helfand MS, Carey MP, Sheri A, Buynak JD, Bonomo RA, Carey PR (2007) Sulbactam forms only minimal amounts of irreversible acrylate-enzyme with SHV-1 beta-lactamase. Biochemistry **46:** 8980-8987

Tricarico D, Mele A, Conte Camerino D (2006) Carbonic anhydrase inhibitors ameliorate the symptoms of hypokalaemic periodic paralysis in rats by opening the muscular Ca2+-activated-K+ channels. Neuromuscul Disord **16:** 39-45

van den Meiracker AH, Man in 't Veld AJ, Fischberg DJ, Molinoff PB, van Eck HJ, Boomsma F, Derkx FH, Schalekamp MA (1988) Acute and long-term effects of acebutolol on systemic and renal hemodynamics, body fluid volumes, catecholamines, active renin, aldosterone, and lymphocyte beta-adrenoceptor density. J Cardiovasc Pharmacol **11:** 413-423

Varet H, Brillet-Gueguen L, Coppee JY, Dillies MA (2016) SARTools: A DESeq2- and EdgeR-Based R Pipeline for Comprehensive Differential Analysis of RNA-Seq Data. PLoS One **11:** e0157022

Vieler A, Wu G, Tsai CH, Bullard B, Cornish AJ, Harvey C, Reca IB, Thornburg C, Achawanantakun R, Buehl CJ, Campbell MS, Cavalier D, Childs KL, Clark TJ, Deshpande R, Erickson E, Armenia Ferguson A, Handee W, Kong Q, Li X, Liu B, Lundback S, Peng C, Roston RL, Sanjaya, Simpson JP, Terbush A, Warakanont J, Zauner S, Farre EM, Hegg EL, Jiang N, Kuo MH, Lu Y, Niyogi KK, Ohlrogge J, Osteryoung KW, Shachar-Hill Y, Sears BB, Sun Y, Takahashi H, Yandell M, Shiu SH, Benning C (2012) Genome, functional gene annotation, and nuclear transformation of the heterokont oleaginous alga Nannochloropsis oceanica CCMP1779. PLoS Genet **8:** e1003064

Walsky RL, Gaman EA, Obach RS (2005) Examination of 209 drugs for inhibition of cytochrome P450 2C8. J Clin Pharmacol **45:** 68-78

Wang JK, Seibert M (2017) Prospects for commercial production of diatoms. Biotechnol Biofuels **10:** 16

Warrilow AG, Martel CM, Parker JE, Melo N, Lamb DC, Nes WD, Kelly DE, Kelly SL (2010) Azole binding properties of Candida albicans sterol 14-alpha demethylase (CaCYP51). Antimicrob Agents Chemother **54:** 4235-4245

Wase N, Tu B, Allen JW, Black P, DiRusso C (2017) Identification and metabolite profiling of chemical activators of lipid accumulation in green algae. Plant Physiol**:** In press

Young MD, Wakefield MJ, Smyth GK, Oshlack A (2010) Gene ontology analysis for RNA-seq: accounting for selection bias. Genome Biol **11:** R14

Zhang JH, Chung TD, Oldenburg KR (1999) A Simple Statistical Parameter for Use in Evaluation and Validation of High Throughput Screening Assays. J Biomol Screen **4:** 67-73

Figure Legends

Figure 1. Calibration of the multiparametric assay for the phenotypic screen. The assay was developed using a strain expressing a Histone H4 protein fused to EYFP (Enhanced Yellow Fluorescent Protein) at the N-terminus. Graphs show the correlations between measured fluorescence and cell concentrations after 48h-incubation in ESAW 1N1P and 0N1P media, respectively. **A. Cell abundance.** The YFP fluorescence was used to evaluate cell abundance in a calibrated population grown in 1N1P medium, by measuring the excitation/emission fluorescence at 515 nm/530 nm. **B. Chlorophyll fluorescence.** The fluorescence of chlorophyll was used as a basic evaluation of cell physiological status, by measuring the excitation/emission fluorescence at 440 nm/680 nm. **C. Nile red fluorescence.** The content in TAG was evaluated by staining with Nile red, measuring the fluorescence at 530nm/580 nm. Data correspond to biological triplicates ± SD. Correlation coefficients were ≤ 0.94. Solid squares, cells grown in 1N1P medium (+ Nitrogen); circles, cells grown in 0NP medium (- Nitrogen).

Figure 2. Multi-parametric screen of the Prestwick Chemical Library. Using the developed assay, *Phaeodactylum tricornutum* cells were incubated 48 hours with compounds of the Prestwick Chemical Library at a final concentration of 10 µM, DMSO 0.5%. Multiple parameters were then measured as described in the Method section. **A. Cell abundance.** The concentration of cells was estimated using a strain expressing a Histone H4 protein fused to EYFP, based on the fluorescence at 515 nm/530 nm. **B. TAG levels.** The content in TAG was evaluated by staining with Nile red, measuring the fluorescence at 530nm/580 nm. **C. Chlorophyll levels.** The fluorescence of chlorophyll was measured at 440 nm/680 nm.

Figure 3. Selection of compounds based on primary and secondary screens. Based on the primary screen, two criteria were used to select compounds for secondary screen: 1) low impact on cell abundance and/or chlorophyll level and 2) increase of Nile Red staining level. **A. Primary screen, correlation between chlorophyll level and cell abundance detection.** Values obtained from chlorophyll fluorescence levels and cell abundance based on YFP fluorescence were plotted. Linear correlation is given by the formula $y = 0.9409x - 2.2011$ ($R^2 = 0.8189$). **B. Primary screen, comparison of Nile Red staining and cell abundance.** Dashed line shows spots corresponding to compounds increasing Nile Red staining above 120 % of average per plate, while maintaining a cell abundance above 50 % of control. **C. Secondary**

screen. Parallel assays were repeated at 10 µM in technical duplicates, using 160 compounds selected following primary screen. Error bars: standard deviation.

Figure 4. Dose-response analyses of secondary screen selected compounds. Dose-response analyses were performed as described in the Methods section, in triplicates, at compound concentrations of 1.5, 3, 6, 12, 25, 50 and 100 µM. Cell abundance was evaluated based on the fluorescence of Histone H4 protein fused to EYFP, and expressed in percentage of untreated control (100% = YFP level at 0 µM compound). TAG accumulation was evaluated based on Nile Red staining, normalized by cell abundance and expressed in percentage of untreated control (100% = Nile Red level per cell at 0 µM compound).

Figure 5. Compounds interfering with sterol metabolism. The pathway is adapted from Fabris et al., 2014. The biosynthesis of isopentenyl-pyrophosphate (isopentenyl-PP) and farnesyl-pyrophosphate (farnesyl-PP), which is common to all isoprenoids, is initiated by the reduction of hydroxymethylglutaryl-CoA (HMG-CoA) into mevalonate. Epoxysqualene is the last non-cyclic intermediate in the pathway. The molecular diversity of sterols is then generated downstream cycloartenol and involves cytochrome P450 cyclooxygenases. The connection with fatty acid (FA) and TAG biosynthesis occurs at the level of acetyl-CoA. FA synthesis is an iterative process adding 2 carbon (2C) per iteration, producing FA of 16 or 18 carbons. FAs can be elongated further in the cytosol and are used for the biosynthesis of polar and storage glycerolipids, including TAG. Inhibitors are shown in red, at the level of their primary enzymatic targets. (?), putative inhibitors in the downstream part of sterol metabolism, acting on cytochrome P450 enzymes. (*), Ro48-8071 effect was described previously by Fabris et al., 2014. Fluorescence imaging of treated wild type cells highlights chlorophyll fluorescence (440 nm / 680 nm) allowing the detection of chloroplasts (Chl) and Nile Red staining (530 nm / 580 nm) of oil droplets enriched in triacylglycerol (TAG). Scale bar, 5 µM.

Figure 6. Glycerolipid profile following treatment with Ethynylestradiol. *Phaeodactylum tricornutum* cells were cultivated in 1N1P medium until a cell density of 1.10^6 cells.mL^{-1} was reached. Cells were then incubated 48 h in presence or absence of compounds, as indicated. Lipids were extracted, separated by TLC, and analyzed as described in Methods. **A, Glycerolipid profiles following treatments with 30 µM Ethynylestradiol and Simvastatin.** Glycerolipids are expressed in nmol per million of cells. **B, Fatty acid profiles of membrane glycerolipids following treatment with 30 µM Ethynylestradiol. C, Fatty acid profile of Triacylglycerol following treatment with 30 µM Ethynylestradiol.** Data correspond to

biological triplicates ± SD. Ethy, Ethynylestradiol; Simva, Simvastatin; DGDG, digalactosyldiacylglycerol; DGTA, diaclyglycerylhydroxymethyl-N,N,N-trimethyl-β-alanine; MGDG, monogalactosyldiacylglycerol; PC, phosphatidylcholine; PG, phosphatidylglycerol; SQDG, sufoquinivosyldiacylglycerol. (*), p-value < 0.05

Figure 7: K-mean clustering of *Phaeodactylum* differentially expressed genes in response to increasing doses of Ethynylestradiol. Only genes being differentially expressed with a |Log2(fold change)| > 1 in at least one of the contrasts (i.e. comparing Ethynylestradiol supplies at 10 µM vs. 0 µM, 20 µM vs. 0 µM or 20 µM vs. 10 µM), and with p-value lower than 0.05, were considered for further analyses. A partition of differentially expressed genes was performed using a K-mean method, with a number of partitions set to 6 and a clustering based on a Euclidian distance (Liu et al., 2014). Two clusters comprise genes downregulated following treatments, *i.e.* group 1 (DR_1) gathering genes with the strongest magnitude in expression decline (in the -2 to -4 Log2FC range) and group 5 (DR_2) with moderate but significant expression decline (Log2FC ~ -1). Four clusters comprise genes upregulated following Ethynylestradiol treatments, *i.e.* groups 2, 3, 4 and 6 (UR_1, UR_2, UR_3 and UR_4, respectively).

Table 1. Compounds selected after secondary screen. Chemical Abstracts Service (CAS) numbers are indicated. Results of the three independent dose-response analyses are compiled, with high-Nile Red (NR) dose-dependent detection and toxicity (*). Previously characterized targets of the selected compounds are classified based on general biological function and/or molecular features.

Chemical name	CAS number	Tertiary screen results (triplicate) and toxicity (*) in the tested concentration range	Previously characterized targets	Known side activities on cytochrome P450 (CYP) involved in sterol metabolism	References
Nucleic acid biosynthesis and cell division					
Pentamidine	140-64-7	High NR in 2/3 tests	Nucleic acid binding activity		(Overington et al., 2006)
Oxytetracycline	6153-64-6	High NR in 2/3 tests	Nucleic acid binding activity		(Overington et al., 2006)
Ifosfamide	3778-73-2	High NR in 2/3 tests	Alkylation of DNA	CYP2B6 (steroid hydroxylase) modulator	(Furlanut and Franceschi, 2003; Chen et al., 2005)
Rifaximin	80621-81-4	High NR in 2/3 tests	RNA polymerase blocking agent		(Overington et al., 2006)
Nocodazole	31430-18-9	High NR in 3/3 tests (> 120%)	Microtubule de-polymerizing agent		(Baas et al., 2016)
Membrane receptors					
Xylometazoline	1218-35-5	High NR in 3/3 tests (> 120%) (*)	Adrenergic receptor agonist		(Haenisch et al., 2010)
Labetalol	32780-64-6	High NR in 2/3 tests	Adrenergic receptor agonist	CYP2D6 (steroid hydroxylase) inhibitor	(Riva et al., 1991; Preissner et al., 2010)
Acebutolol	34381-68-5	High NR in 2/3 tests	Adrenergic receptor agonist	CYP2D6 (steroid hydroxylase) inhibitor	(van den Meiracker et al., 1988; Preissner et al., 2010)
Meclozine	1104-22-9	High NR in 2/3 tests	Dopamine (precursor of adrenaline) antagonist		(Haraguchi et al., 1997)
Serotonin	153-98-0	High NR in 2/3 tests	Serotonin receptor ligand		(Pytliak et al., 2011)
Alverine	5560-59-8	High NR in 3/3 tests (> 120%) (*)	Serotonin receptor antagonist		(Coelho et al., 2001)
Pirenperone	75444-65-4	High NR in 2/3 tests	Serotonin receptor antagonist		(Pawlowski et al., 1985)
Hyoscyamine	101-31-5	High NR in 2/3 tests	Acetylcholine receptor antagonist		(Huang et al., 1998)
Pipenzolate	125-51-9	High NR in 2/3 tests	Acetylcholine receptor antagonist		(Attwood, 1976)
Mecamylamine	826-39-1	High NR in 2/3 tests	Acetylcholine receptor antagonist		(Overington et al., 2006)
Bephenium	3818-50-6	High NR in 2/3 tests	Acetylcholine receptor antagonist		(Qian et al., 2006)
Dimaprit	23256-33-9	High NR in 2/3 tests	Histamine (2-(1H-imidazol-4-yl)ethanamine) H2 receptor antagonist		(Shteinikov et al., 2017)
Membrane transporters					
Bendroflumethiazide	73-48-3	High NR in 2/3 tests	Solute carrier family 12 member 3 inhibitor / Carbonic anhydrase inhibitor		(Chen et al., 2002; Tricarico et al., 2006)
Rimantadine	13392-28-4	High NR in 3/3 tests (> 120%) (*)	Proton pump inhibitor		(Imming et al., 2006)
Gaboxadol	64603-91-4		Proton-coupled amino acid transporter		(Larsen et al., 2010)
Antimycin A	1397-94-0	High NR in 3/3 tests (> 120%)	Mitochondria or chloroplast electron transport chains		(Shikanai, 2014; Georgakopoulos et al., 2017)
Sterol metabolism					
Estrone	53-16-7	High NR in 2/3 tests	CYP2B6 (steroid hydroxylase) substrate		(Preissner et al., 2010)
Ethynylestradiol	57-63-6	High NR in 3/3 tests (>120 %)	CYP2C8 (steroid hydroxylase) inhibitor		(Walsky et al., 2005)
Mevastatin	73573-88-3	High NR in 3/3 tests (> 120%)	HMG-CoA reductase	CYP2C8 (steroid hydroxylase) inhibitor	(Chen et al., 2002; Tornio et al., 2005)
Simvastatin	79902-63-9	High NR in 3/3 tests (> 120%) (*)	HMG-CoA reductase	CYP2C8 (steroid hydroxylase) inhibitor	(Liu et al., 2003; Tornio et al., 2005)
Ketoconazole	65277-42-1	High NR in 2/3 tests	CYP (sterol 14-alpha demethylase) inhibitor		(Warrilow et al., 2010)
Cyclic nucleotide signaling					
Zardaverine	101975-10-4	High NR in 2/3 tests	Cyclic nucleotide phosphodiesterase inhibitor		(Schudt et al., 1991)
Trapidil	15421-84-8	High NR in 2/3 tests	Cyclic nucleotide phosphodiesterase inhibitor		(Somuncu et al., 2005)
Oxilipin signaling					
Meloxicam	71125-38-7	High NR in 2/3 tests	Prostanoid signaling modulator / Cyclo-oxygenase COXII / prostaglandine-endoperoxyde synthase inhibitor	CYP2C9 (steroid hydroxylase) inhibitor	(Chesne et al., 1998; Panara et al., 1999)
Azapropazone	13539-59-8	High NR in 2/3 tests	Prostanoid signaling modulator / Cyclo-oxygenase COXII / prostaglandine-endoperoxyde synthase inhibitor		(Priddy et al., 1990)
Misoprostol	59122-46-2	High NR in 2/3 tests	Prostaglandin E1 analog / Prostaglandin receptor agonist		(Nataraj et al., 2001)
Enzymes (carbohydrate metabolism, purine catabolism and/or beta-lactam drug resistance)					
Miglitol	72432-03-2	High NR in 2/3 tests	Alpha-glycosidase inhibitor		(Fukaya et al., 2009)
Flucloxacillin	1847-24-1	High NR in 2/3 tests	Penicillin (beta-lactam drug) binding protein (glycosyltransferase) inhibitor		(Mainardi et al., 2008)
Sulbactam	68373-14-8	High NR in 2/3 tests	Beta-lactamase inhibitor		(Totir et al., 2007)
Allopurinol	315-30-0	High NR in 3/3 tests (> 120%)	Inhibition of xanthine (imidazole derived heterocycle) oxidase		(Pacher et al., 2006)

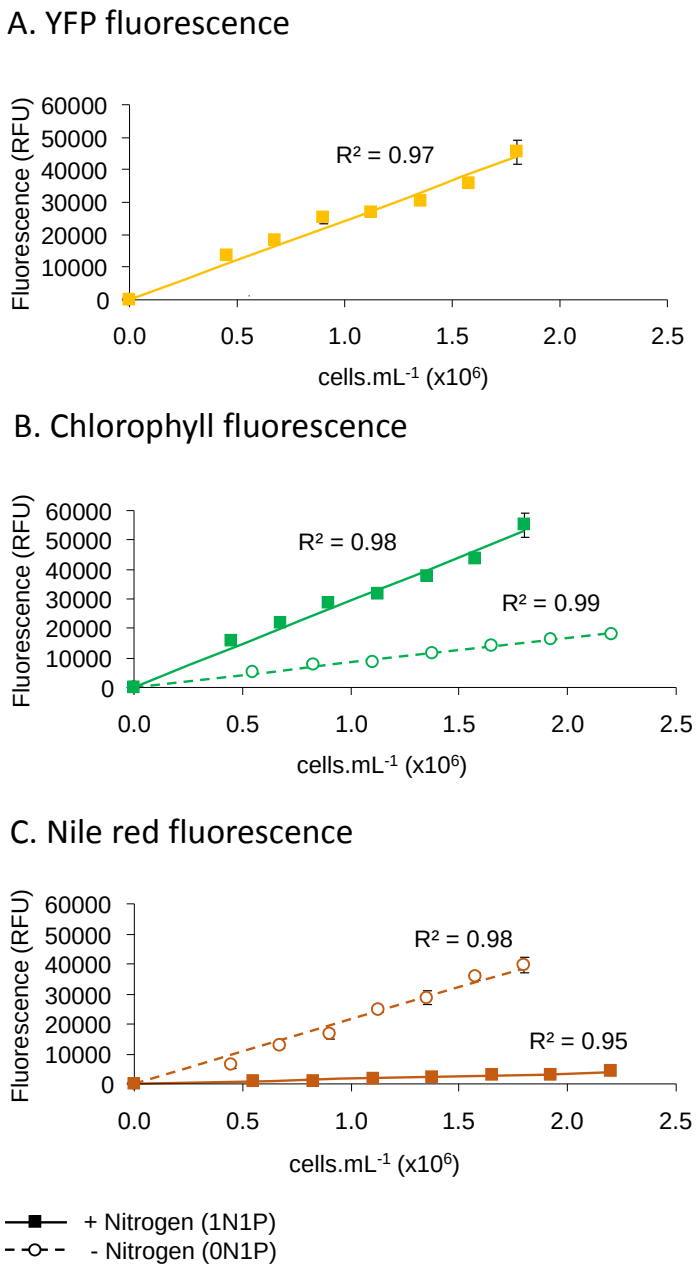

Figure 1. Calibration of the multiparametric assay for the phenotypic screen. The assay was developed using a strain expressing a Histone H4 protein fused to EYFP (Enhanced Yellow Fluorescent Protein) at the N-terminus. Graphs show the correlations between measured fluorescence and cell concentrations after 48h-incubation in ESAW 1N1P and 0N1P media, respectively. **A. Cell abundance.** The YFP fluorescence was used to evaluate cell abundance in a calibrated population grown in 1N1P medium, by measuring the excitation/emission fluorescence at 515 nm/530 nm. **B. Chlorophyll fluorescence.** The fluorescence of chlorophyll was used as a basic evaluation of cell physiological status, by measuring the excitation/emission fluorescence at 440 nm/680 nm. **C. Nile red fluorescence.** The content in TAG was evaluated by staining with Nile red, measuring the fluorescence at 530nm/580 nm. Data correspond to biological triplicates ± SD. Correlation coefficients were ≤ 0.94. Solid squares, cells grown in 1N1P medium (+ Nitrogen); circles, cells grown in 0NP medium (- Nitrogen).

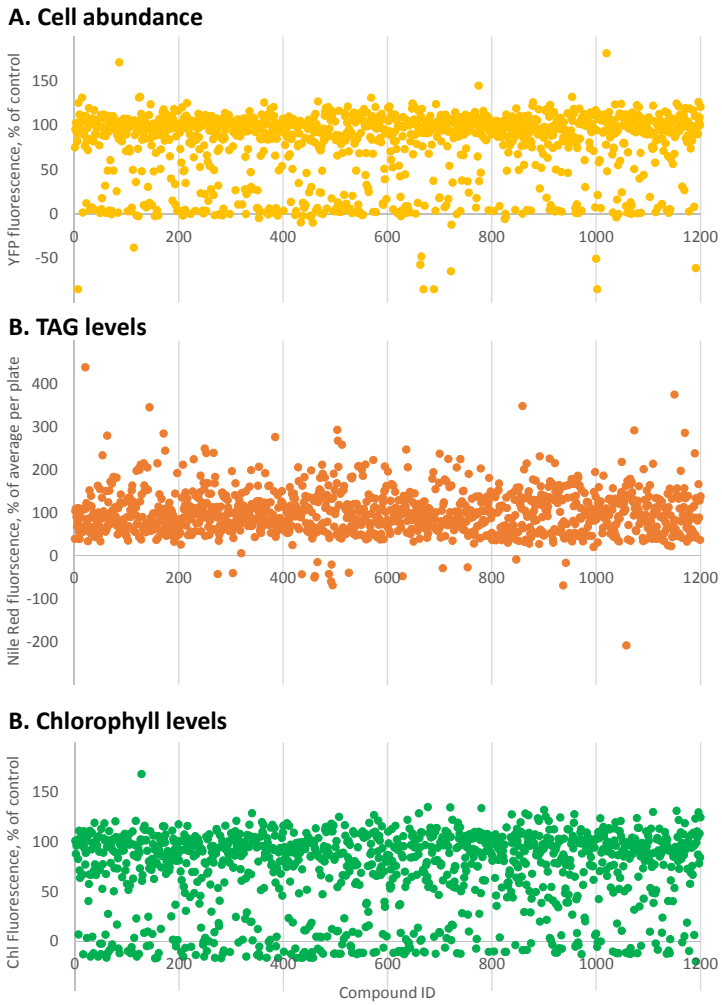

Figure 2. Multi-parametric screen of the Prestwick Chemical Library. Using the developed assay, *Phaeodactylum tricornutum* cells were incubated 48 hours with compounds of the Prestwick Chemical Library at a final concentration of 10 µM, DMSO 0.5%. Multiple parameters were then measured as described in the Method section. **A. Cell abundance.** The concentration of cells was estimated using a strain expressing a Histone H4 protein fused to EYFP, based on the fluorescence at 515 nm/530 nm. **B. TAG levels.** The content in TAG was evaluated by staining with Nile red, measuring the fluorescence at 530nm/580 nm. **C. Chlorophyll levels.** The fluorescence of chlorophyll was measured at 440 nm/680 nm.

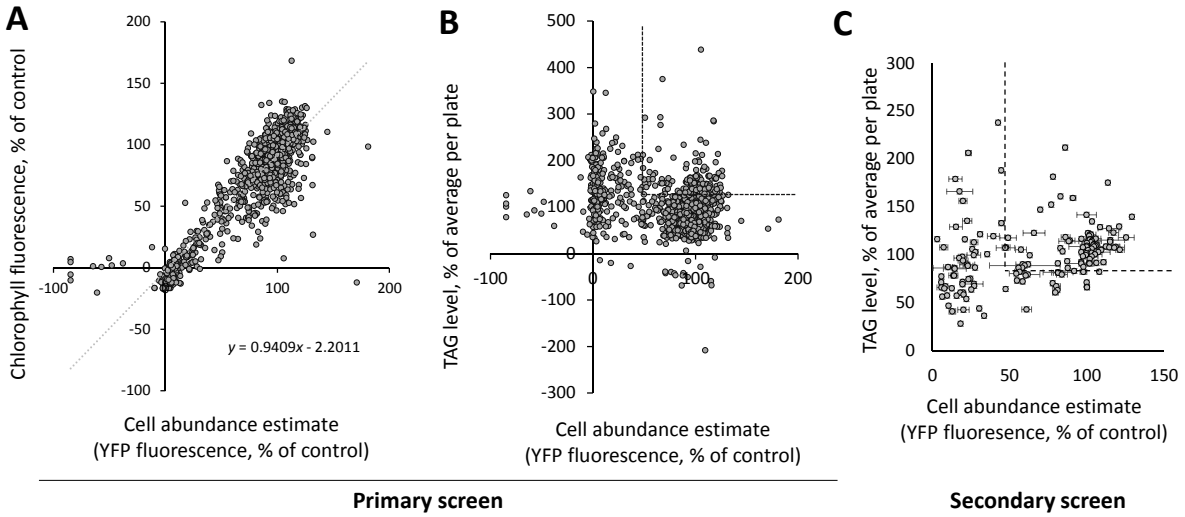

Figure 3. Selection of compounds based on primary and secondary screens. Based on the primary screen, two criteria were used to select compounds for secondary screen: 1) low impact on cell abundance and/or chlorophyll level and 2) increase of Nile Red staining level. **A. Primary screen, correlation between chlorophyll level and cell abundance detection.** Values obtained from chlorophyll fluorescence levels and cell abundance based on YFP fluorescence were plotted. Linear correlation is given by the formula $y = 0.9409x - 2.2011$ ($R^2 = 0.8189$). **B. Primary screen, comparison of Nile Red staining and cell abundance.** Dashed line shows spots corresponding to compounds increasing Nile Red staining above 120 % of average per plate, while maintaining a cell abundance above 50 % of control. **C. Secondary screen.** Parallel assays were repeated at 10 µM in technical duplicates, using 160 compounds selected following primary screen. Error bars: standard deviation.

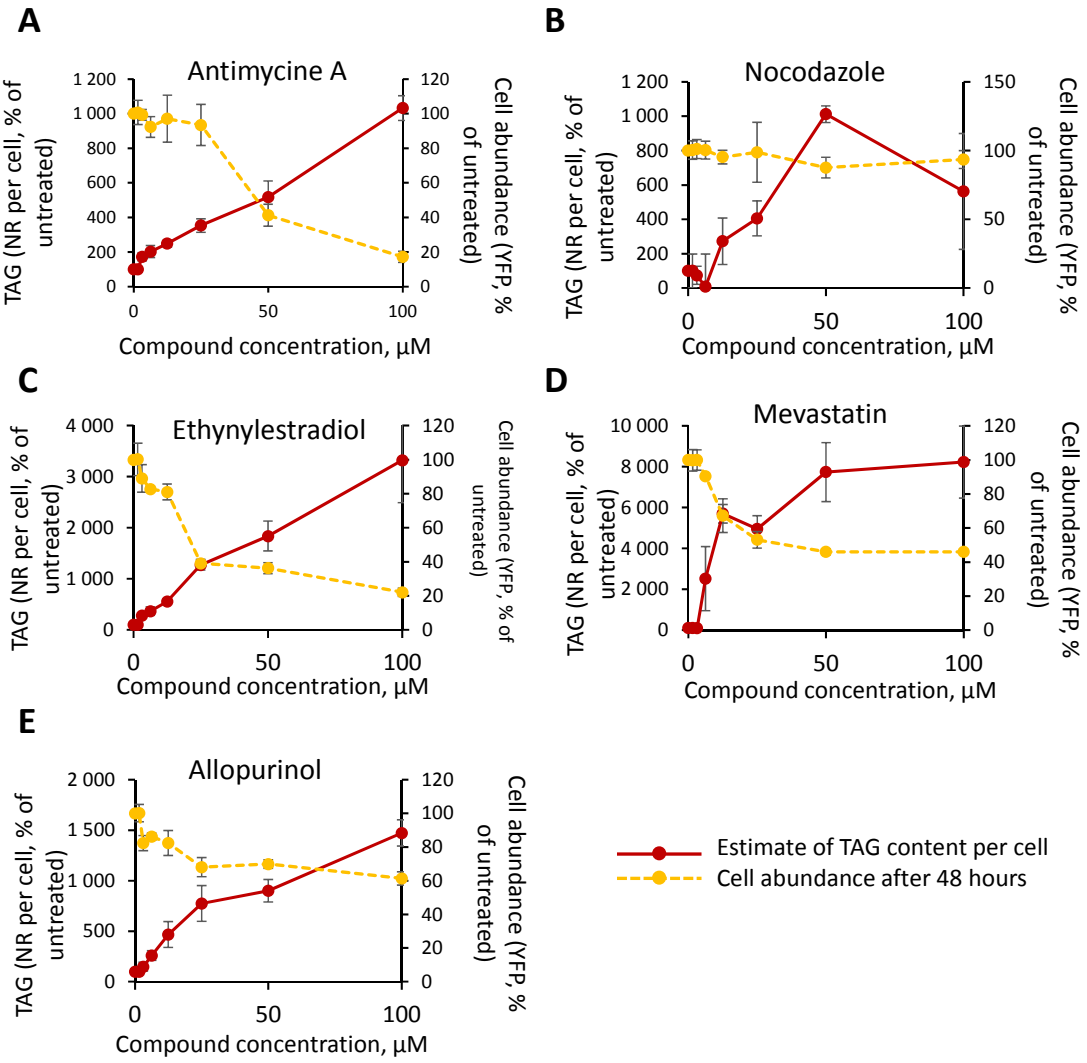

Figure 4. Dose-response analyses of secondary screen selected compounds. Dose-response analyses were performed as described in the Methods section, in triplicates, at compound concentrations of 1.5, 3, 6, 12, 25, 50 and 100 µM. Cell abundance was evaluated based on the fluorescence of Histone H4 protein fused to EYFP, and expressed in percentage of untreated control (100% = YFP level at 0 µM compound). TAG accumulation was evaluated based on Nile Red staining, normalized by cell abundance and expressed in percentage of untreated control (100% = Nile Red level per cell at 0 µM compound).

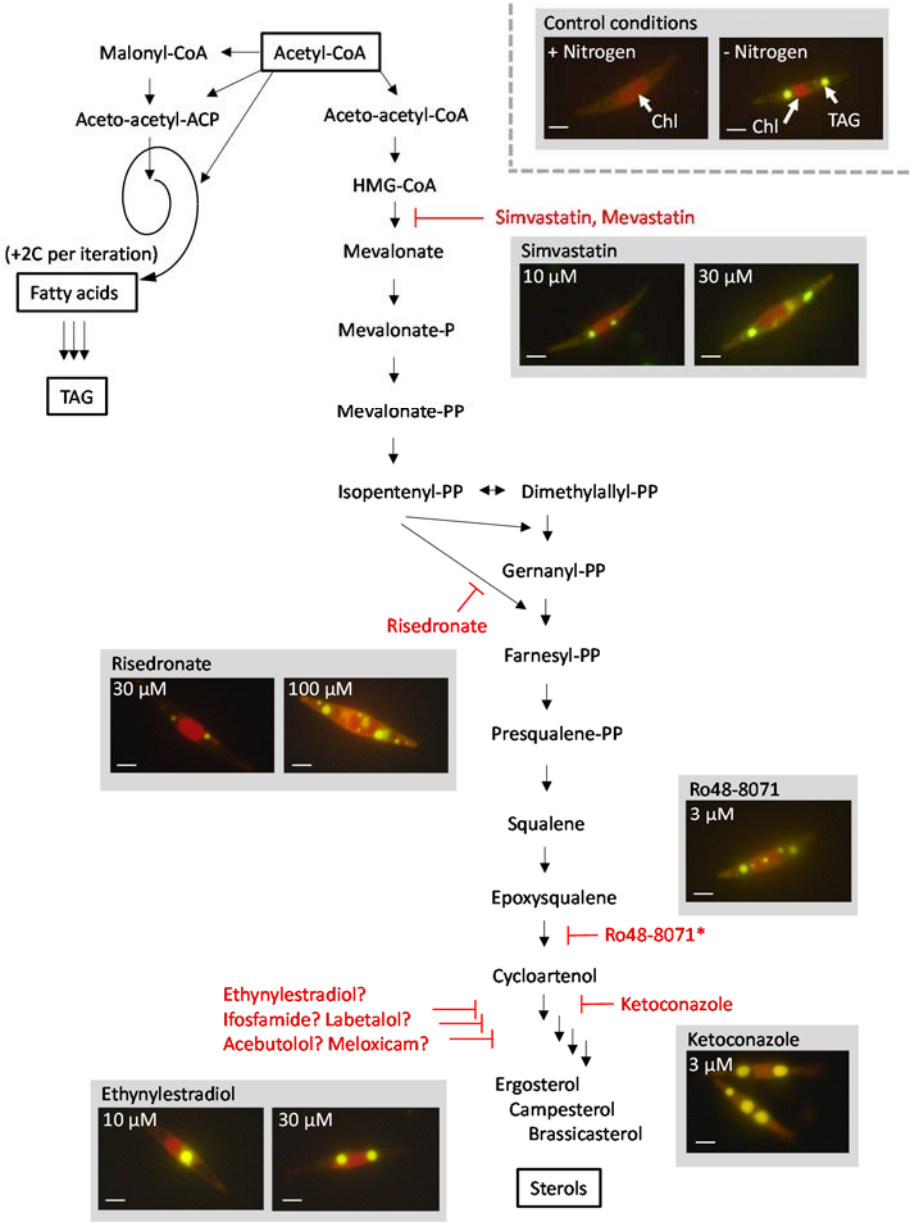

Figure 5. Compounds interfering with sterol metabolism. The pathway is adapted from Fabris et al., 2014. The biosynthesis of isopentenyl-pyrophosphate (isopentenyl-PP) and farnesyl-pyrophosphate (farnesyl-PP), which is common to all isoprenoids, is initiated by the reduction of hydroxymethylglutaryl-CoA (HMG-CoA) into mevalonate. Epoxysqualene is the last non-cyclic intermediate in the pathway. The molecular diversity of sterols is then generated downstream cycloartenol and involves cytochrome P450 cyclooxygenases. The connection with fatty acid (FA) and TAG biosynthesis occurs at the level of acetyl-CoA. FA synthesis is an iterative process adding 2 carbon (2C) per iteration, producing FA of 16 or 18 carbons. FAs can be elongated further in the cytosol and are used for the biosynthesis of polar and storage glycerolipids, including TAG. Inhibitors are shown in red, at the level of their primary enzymatic targets. (?), putative inhibitors in the downstream part of sterol metabolism, acting on cytochrome P450 enzymes. (*), Ro48-8071 effect was described previously by Fabris et al., 2014. Fluorescence imaging of treated wild type cells highlights chlorophyll fluorescence (440 nm / 680 nm) allowing the detection of chloroplasts (Chl) and Nile Red staining (530 nm / 580 nm) of oil droplets enriched in triacylglycerol (TAG). Scale bar, 5 µM.

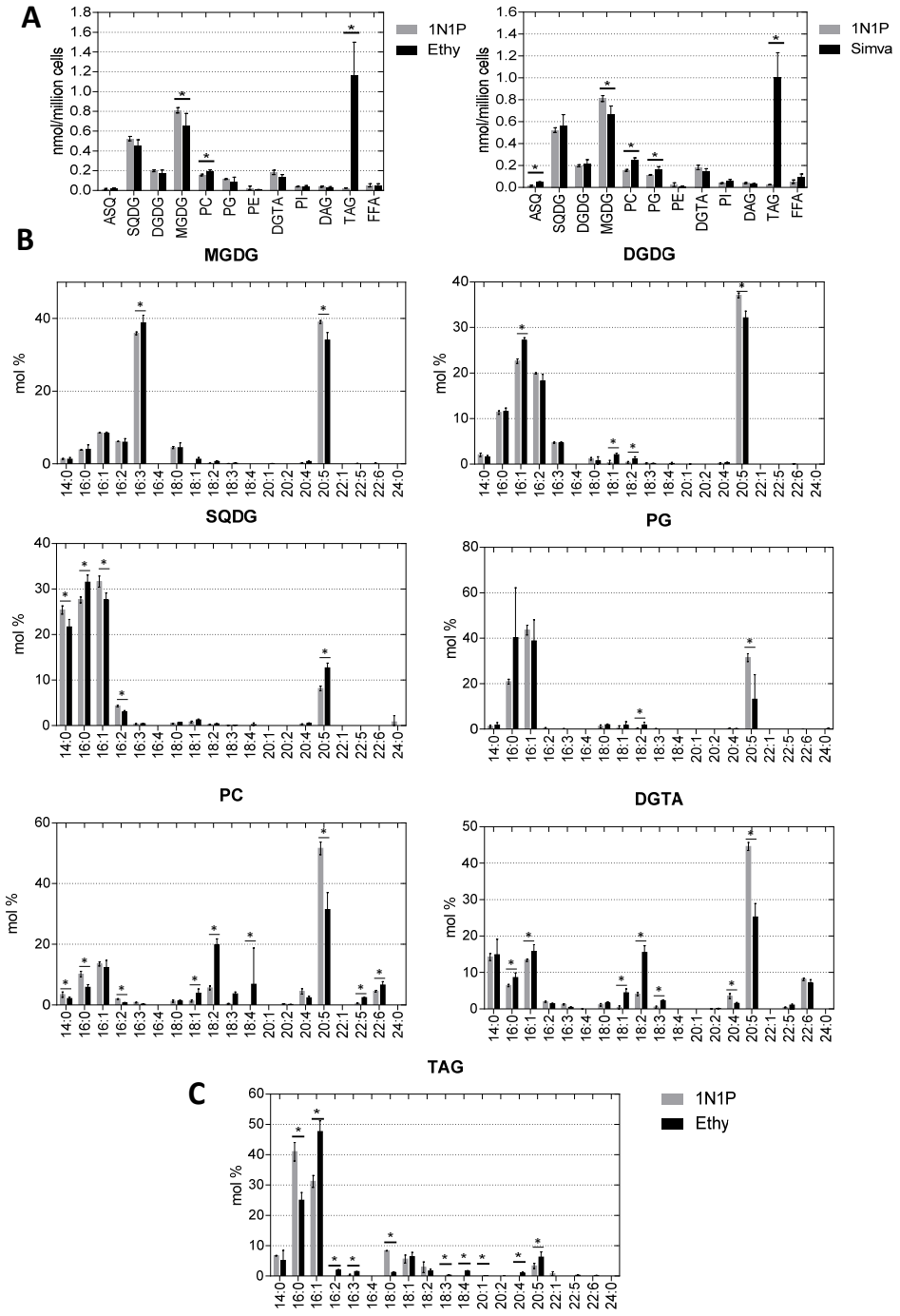

Figure 6. Glycerolipid profile following treatment with Ethynylestradiol. *Phaeodactylum tricornutum* cells were cultivated in 1N1P medium until a cell density of 1.10^6 cells.mL^{-1} was reached. Cells were then incubated 48 h in presence or absence of compounds, as indicated. Lipids were extracted, separated by TLC, and analyzed as described in Methods. **A, Glycerolipid profiles following treatments with 30 µM Ethynylestradiol and Simvastatin.** Glycerolipids are expressed in nmol per million of cells. **B, Fatty acid profiles of membrane glycerolipids following treatment with 30 µM Ethynylestradiol. C, Fatty acid profile of Triacylglycerol following treatment with 30 µM Ethynylestradiol.** Data correspond to biological triplicates ± SD. Ethy, Ethynylestradiol; Simva, Simvastatin; DGDG, digalactosyldiacylglycerol; DGTA, diaclyglycerylhydroxymethyl-N,N,N-trimethyl-β-alanine; MGDG, monogalactosyldiacylglycerol; PC, phosphatidylcholine; PG, phosphatidylglycerol; SQDG, sufoquinivosyldiacylglycerol. (*), p-value < 0.05

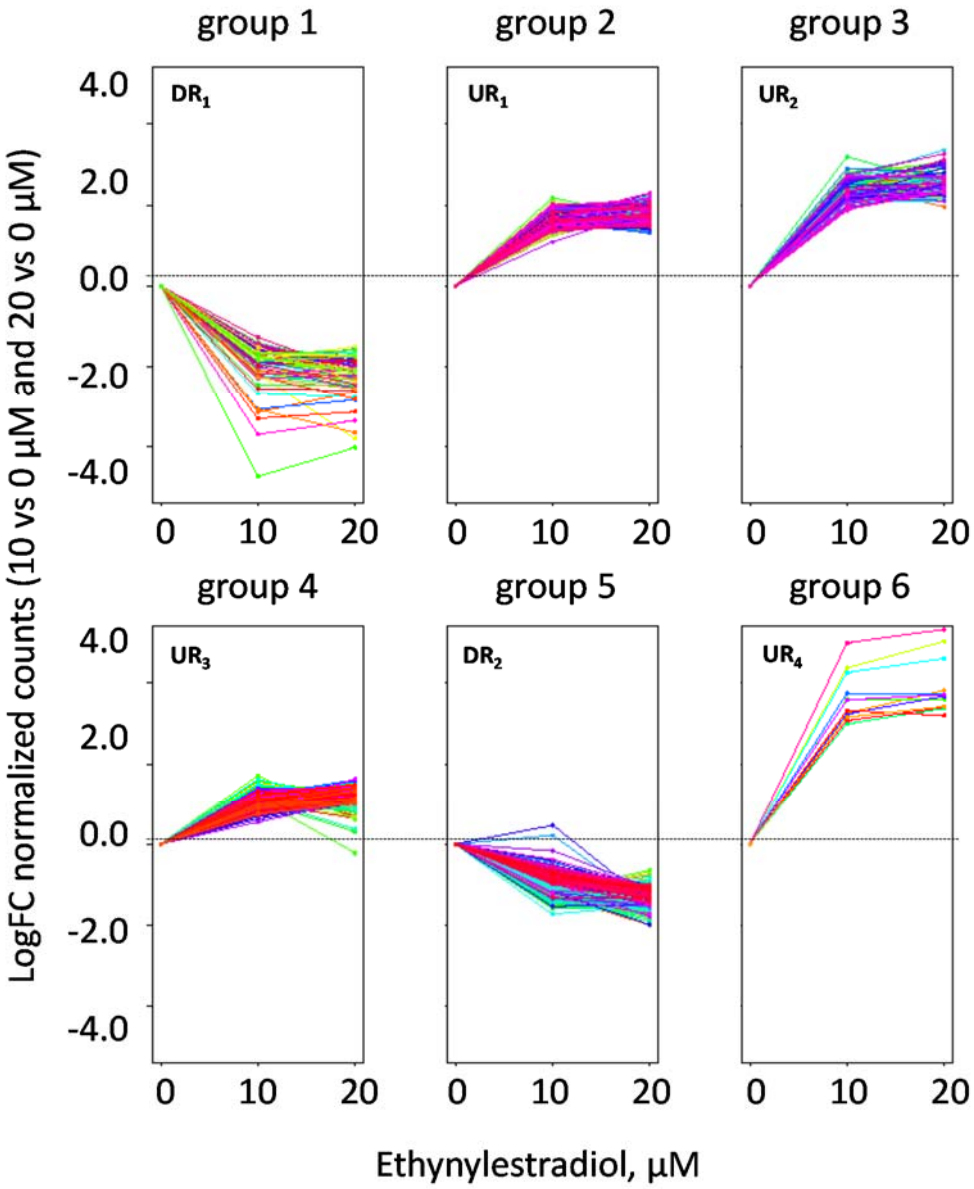

Figure 7: K-mean clustering of *Phaeodactylum* differentially expressed genes in response to increasing doses of Ethynylestradiol. Only genes being differentially expressed with a |Log2(fold change)| > 1 in at least one of the contrasts (i.e. comparing Ethynylestradiol supplies at 10 µM vs. 0 µM, 20 µM vs. 0 µM or 20 µM vs. 10 µM), and with p-value lower than 0.05, were considered for further analyses. A partition of differentially expressed genes was performed using a K-mean method, with a number of partitions set to 6 and a clustering based on a Euclidian distance (Liu et al., 2014). Two clusters comprise genes downregulated following treatments, *i.e.* group 1 (DR_1) gathering genes with the strongest magnitude in expression decline (in the -2 to -4 Log2FC range) and group 5 (DR_2) with moderate but significant expression decline (Log2FC ~ -1). Four clusters comprise genes upregulated following Ethynylestradiol treatments, *i.e.* groups 2, 3, 4 and 6 (UR_1, UR_2, UR_3 and UR_4, respectively).